

# GradMetaNet: An Equivariant Architecture for Learning on Gradients

**Yoav Gelberg\***

University of Oxford

yoav@robots.ox.ac.uk

**Yam Eitan\***

Technion

yam.eitan@campus.technion.ac.il

**Aviv Navon**

Independent Reseracher

**Aviv Shamsian**

Bar-Ilan University

**Theo (Moe) Putterman**

UC Berkeley

**Michael Bronstein**

University of Oxford, AITHYRA

**Haggai Maron**

Technion/NVIDIA

## Abstract

Gradients of neural networks encode valuable information for optimization, editing, and analysis of models. Therefore, practitioners often treat gradients as inputs to task-specific algorithms, e.g. for pruning or optimization. Recent works explore *learning* algorithms that operate directly on gradients but use architectures that are not specifically designed for gradient processing, limiting their applicability. In this paper, we present a principled approach for designing architectures that process gradients. Our approach is guided by three principles: (1) equivariant design that preserves neuron permutation symmetries, (2) processing sets of gradients across multiple data points to capture curvature information, and (3) efficient gradient representation through rank-1 decomposition. Based on these principles, we introduce GradMetaNet, a novel architecture for learning on gradients, constructed from simple equivariant blocks. We prove universality results for GradMetaNet, and show that previous approaches cannot approximate natural gradient-based functions that GradMetaNet can. We then demonstrate GradMetaNet’s effectiveness on a diverse set of gradient-based tasks on MLPs and transformers, such as learned optimization, INR editing, and estimating loss landscape curvature.

## 1 Introduction

Gradients of neural networks are fundamental objects in deep learning, driving optimization and offering insights into model behavior. Beyond gradient descent and its variants [9, 40, 70], gradients are used in diverse applications that call for sophisticated processing. These applications broadly span three areas: model optimization, editing, and analysis. In accelerated **optimization**, several approaches use (multi-)gradient information to improve convergence speed. These approaches range from classical curvature-aware methods like natural gradient descent [3] powered by efficient approximate curvature-based preconditioners [25, 27, 29, 49, 55, 85], to learned optimizers [6, 8, 56]. In model **editing**, gradient information guides pruning algorithms for weight compression [32, 45, 82, 87], and enables targeted behavior modification in large language models [18, 58]. For model **analysis** and interpretability, gradient information is used to compute influence functions that trace the impact of individual training samples [28, 42], estimate model uncertainty [17, 36], and more.

While most approaches rely on predefined algorithms and heuristics, recent works explore *learnable* processing of gradients for downstream tasks [18, 41, 58, 91]. Learned methods offer two key

\*Equal contribution

advantages. First, they are essential when no predefined algorithm is known. In model editing for instance, updating a model using gradients of the editing objective while maintaining performance on a validation set, requires intricate gradient adaptations that are difficult to model analytically. Learned approaches can effectively discover these gradient adaptations through supervision [18, 58]. Second, learned approaches offer a powerful mechanism for approximating computationally expensive methods. Methods such as natural gradient descent require hand-crafted approximations for practical application. Learned approaches, if successful, can bridge this gap by discovering efficient approximations tailored for a specific distribution of models. Unfortunately, existing learned approaches use architectures not specifically designed for processing *gradient information*. For example, De Cao et al. [18], Mitchell et al. [58] don’t account for the parameter symmetries in the gradient representation (as they process gradients of a single model), while recent weight-space methods [41, 91] use inefficient gradient representations and process only a single gradient. As a result, they are unable to capture curvature information that is critical to many tasks.

**Our approach.** In this paper, we introduce GradMetaNet, an architecture designed for learning on gradients of deep models such as *MLPs* and *transformers*. GradMetaNet’s design is guided by the following principles: (1) **Respecting symmetries:** Neural parameter spaces exhibit inherent symmetries, leading to redundancies in gradient representations. GradMetaNet’s design is derived to respect these symmetries, reducing the number of parameters and improving sample efficiency. As demonstrated in previous work [11, 12, 16, 22, 43, 47, 78, 90], equivariant design is crucial for learning on data with symmetries. (2) **Processing sets of gradients:** Many applications, such as curvature-aware optimization, pruning, and uncertainty estimation, require access to *collections* of gradients on different datapoints which encode the local geometry of the loss. GradMetaNet is thus designed to efficiently handle sets of gradients computed on different datapoints. (3) **Efficient representation:** As gradients are extremely high-dimensional, we encode them efficiently. Gradients of neural networks, evaluated on a single data point, admit a rank-1 decomposition which provides a compact representation that scales linearly (rather than quadratically) with the number of neurons.

Decomposed gradients have a simpler symmetry structure compared to the raw weight representation, allowing us to construct GradMetaNet using simple equivariant building blocks [31, 75, 90] and to incorporate attention mechanisms. This enables us to prove universality results still unknown for weight-space models. Additionally, we formally demonstrate the necessity of processing sets of gradients, proving that several fundamental gradient-based algorithms cannot be approximated based on a single averaged gradient.

We evaluate GradMetaNet on several gradient learning tasks, comparing to equivariant weight-space architectures and other natural baselines. First, we demonstrate GradMetaNet’s ability to predict local curvature information using a small sample of gradients, achieving a 26.3% improvement over standard approximations, and outperforming other learned approaches. We then integrate GradMetaNet into learned optimizer architectures and apply it to train image classifiers and transformer language models, achieving up to a 4.63 $\times$  reduction in steps compared to Adam, and a 1.78 $\times$  improvement over other learned baselines. Finally, we use GradMetaNet for model editing, where we improve on current **state-of-the-art** results in editing MNIST and CIFAR10 INRs by up-to 22.5%. Across all tasks, GradMetaNet consistently outperforms baselines, highlighting the value of efficient gradient representations and equivariant processing of sets of gradients.

## 2 Related Work

Several recent works have explored methods for learning over neural network weights [5, 20, 34, 35, 37, 41, 48, 60, 61, 66, 72–74, 81, 91, 92]. These methods often use equivariant architectures [7, 13, 15, 22, 24, 43, 47, 53, 67, 68, 71, 86, 90] that respect the internal symmetry of neural

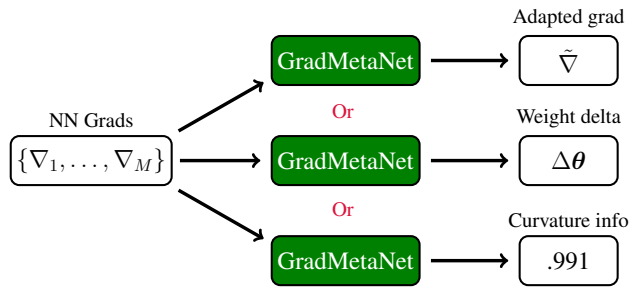


Figure 1: We propose GradMetaNet, a novel architecture that processes sets of gradients and can learn to compute gradient adaptations, parameter edits, or scalar values such as curvature information or influence functions.

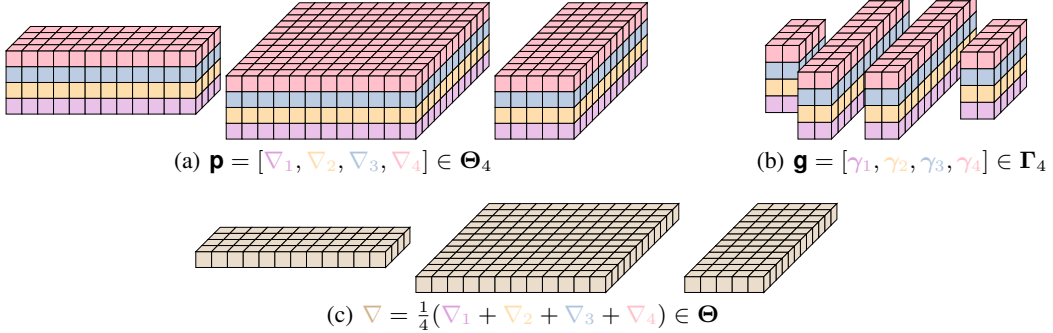


Figure 2: Gradient information on a batch of datapoints in different tensor representations. In 2(a) a stack of the weight-shaped gradients, one for each datapoint. In 2(b) a stack of the rank-1 gradient decompositions. In 2(c) the gradient of the average loss on the batch. All of these tensors are naturally computed when backpropagating the loss on the batch. GradMetaNet process tensors  $\mathbf{g} \in \Gamma_b$ .

network weight spaces. A particularly promising application is processing gradients in weight space for tasks such as learned optimization [41, 91]. While these approaches respect the natural symmetries of gradients, they typically operate on a single gradient, missing valuable information encoded in gradient statistics. Furthermore, these methods process high-dimensional, full-size gradients limiting scalability. Other works, such as De Cao et al. [18], Mitchell et al. [58], analyze gradients of a *fixed* pre-trained model, and are not suitable for settings involving different models or evolving parameter configurations (e.g. learned optimization), as they are not equivariant to permutation symmetries.

Among classical, non-learned approaches, methods such as K-FAC and its variants [25, 27, 55], offer efficient ways to extract curvature-information from gradients. These methods, widely used for curvature-aware optimization [25, 27, 29, 49, 55, 85], pruning [82, 87], uncertainty estimation [17, 36], and influence function estimation [28], need to make probabilistic assumptions on the distribution of gradients for computational feasibility. We advance this perspective by introducing a *learnable* approach to modeling these gradient distributions using GradMetaNet, offering greater flexibility and expressiveness.

### 3 Background

**Notation.** Throughout the paper, we denote models by  $\mathbf{f}_\theta : \mathcal{X} \rightarrow \mathcal{Y}$ , where  $\theta \in \Theta$  are the parameters. When  $\mathbf{f}_\theta$  is a multi-layer perceptron (MLP), we write the input dimension as  $d_0$ , the output dimension as  $d_L$ , the hidden dimensions as  $d_1, \dots, d_{L-1}$ , and denote the activation function by  $\sigma$ . In this case, the parameters are given by  $\theta = (\mathbf{W}_1, \mathbf{b}_1, \dots, \mathbf{W}_L, \mathbf{b}_L)$ . Given a dataset  $\mathcal{D} \subseteq \mathcal{X} \times \mathcal{Y}$ , a loss function  $\ell : \mathcal{Y} \times \mathcal{Y} \rightarrow \mathbb{R}$ , and a batch  $\mathcal{B} \subseteq \mathcal{D}$ , we denote the loss on the batch by

$$\mathcal{L}_{\mathcal{B}}(\theta) := \frac{1}{|\mathcal{B}|} \sum_{(\mathbf{x}, \mathbf{y}) \in \mathcal{B}} \ell(\mathbf{f}_\theta(\mathbf{x}), \mathbf{y}).$$

The parameters gradients of the loss on the batch are denoted by  $\nabla_{\mathcal{B}} := \nabla_{\theta} \mathcal{L}_{\mathcal{B}}(\theta)$ . For a single data point  $(\mathbf{x}, \mathbf{y})$ , we write  $\mathcal{L}_{(\mathbf{x}, \mathbf{y})}(\theta) := \ell(\mathbf{f}_\theta(\mathbf{x}), \mathbf{y})$  and  $\nabla_{(\mathbf{x}, \mathbf{y})} := \nabla_{\theta} \mathcal{L}_{(\mathbf{x}, \mathbf{y})}(\theta)$ .

**Rank-1 decomposition of gradients.** While general parameter gradients have the same shape as parameters, for many neural architectures, the gradient  $\nabla_{(\mathbf{x}, \mathbf{y})}$  admits a rank-1 decomposition through the computation graph of  $\mathbf{f}_\theta$ . For an MLP  $\mathbf{f}_\theta$ , let  $\mathbf{a}^{(l)}$  and  $\mathbf{u}^{(l)}$  denote  $\mathbf{x}$ 's activation and pre-activation vectors at layer  $l$ . The backpropagated signal (pre-activation gradient) at layer  $l$  is

$$\mathbf{g}^{(l)} := \frac{\partial \mathcal{L}_{(\mathbf{x}, \mathbf{y})}(\theta)}{\partial \mathbf{u}^{(l)}} = \frac{\partial \ell(\mathbf{f}_\theta(\mathbf{x}), \mathbf{y})}{\partial \mathbf{u}^{(l)}}. \quad (1)$$

Applying the chain rule yields the following expressions for the weight and bias gradients:

$$\nabla_{\mathbf{W}_l} \mathcal{L}_{(\mathbf{x}, \mathbf{y})}(\theta) = \mathbf{g}^{(l)} (\mathbf{a}^{(l-1)})^\top, \quad \nabla_{\mathbf{b}_l} \mathcal{L}_{(\mathbf{x}, \mathbf{y})}(\theta) = \mathbf{g}^{(l)}. \quad (2)$$

See full derivation in Appendix A.1. This decomposition allows us to represent  $\nabla_{(\mathbf{x}, \mathbf{y})}$  using the tuple  $(\gamma^{(0)}, \dots, \gamma^{(L)})$ , where  $\gamma^{(l)} := (\mathbf{a}^{(l)}, \mathbf{g}^{(l)})$ . Note that  $\mathbf{a}^{(l)}$  and  $\mathbf{g}^{(l)}$  are naturally computed during backpropagation, so they can be extracted *without additional cost*, e.g. using hooks in standard frameworks like PyTorch [65]. See code example in Appendix A.2.

**Decomposition for transformer gradients.** Similar gradient decompositions exists for many other neural architectures [21, 27]. In Appendix B.1 we derive such a decomposition for *all components of the transformer*. To illustrate the structure of the decomposition, we focus here on the feedforward (MLP) layers, which account for the majority of parameters. Given an input sequence  $\mathbf{s} = (x_1, \dots, x_T)$ , let  $\mathbf{a}_t^{(l)}$  denote the activation of token  $x_t$  at layer  $l$  of the MLP component in a transformer block, and let  $\mathbf{g}_t^{(l)}$  be the corresponding pre-activation gradient signal, computed with respect to the loss on the *entire sequence*  $\mathcal{L}_s(\theta)$ . We similarly get:

$$\nabla_{\mathbf{W}_l} \mathcal{L}_s(\theta) = \sum_{t=1}^T \mathbf{g}_t^{(l)} (\mathbf{a}_t^{(l-1)})^\top, \quad \nabla_{\mathbf{b}_l} \mathcal{L}_s(\theta) = \sum_{t=1}^T \mathbf{g}_t^{(l)}. \quad (3)$$

We can therefore represent the gradient using  $\gamma_1^{(l)}, \dots, \gamma_T^{(l)}$  where  $\gamma_t^{(l)} := (\mathbf{a}_t^{(l)}, \mathbf{g}_t^{(l)})$ . In other words, while we incur an additional sequence dimension, the rank-1 decomposition still holds per-token.

**Approximate curvature from gradient statistics.** Gradients statistics across datapoints encode information about the local geometry of the loss landscape. For example, the Fisher information matrix (FIM)

$$\mathbf{F}_\theta = \mathbb{E}_{\substack{\mathbf{x} \sim \mathcal{D}, \\ \mathbf{y} \sim p_\theta(\mathbf{y}|\mathbf{x})}} (\nabla_\theta \log(p_\theta(\mathbf{y}|\mathbf{x})) \nabla_\theta \log(p_\theta(\mathbf{y}|\mathbf{x}))^\top)$$

is a second order approximation of the change in the model’s predictive distribution  $p_\theta(\mathbf{y}|\mathbf{x})$  with respect to a change in the parameters, and when  $\theta$  is a local minimum, the FIM is identical to the Hessian. Gradient decompositions similar to the one discussed above have been used to derive tractable approximation of the FIM [25, 27, 29, 49, 55, 85]. In this work we directly process sets of gradients to enable learning the local geometry of the loss landscape from their statistics. For background on the Fisher Information Matrix see Appendix A.3 and for a detailed overview refer to Martens [54], Pascanu [64].

## 4 Symmetries of Decomposed Gradients

**Weight-space symmetries.** Many neural architectures exhibit parameter space symmetries: parameter transformations that leave the network’s function unchanged. In particular, MLPs exhibit well-documented permutation invariance [1, 33, 60, 76, 92]: permuting the neurons of a hidden layer, while keeping track of the connections to the neighboring layers, alters the weight matrices but preserves the function represented by the network. This parameter space symmetry can be expressed by an action of the permutation symmetry group  $G := S_{d_1} \times \dots \times S_{d_{L-1}}$ . For  $\theta = (\mathbf{W}_1, \mathbf{b}_1, \dots, \mathbf{W}_L, \mathbf{b}_L) \in \Theta$  and  $h = (\tau_1, \dots, \tau_{L-1}) \in G$ , the action  $h \cdot \theta = (\mathbf{W}'_1, \mathbf{b}'_1, \dots, \mathbf{W}'_L, \mathbf{b}'_L)$  is given by

$$\begin{aligned} \mathbf{W}'_1 &= \mathbf{P}_{\tau_1}^\top \mathbf{W}_1, & \mathbf{b}'_1 &= \mathbf{P}_{\tau_1}^\top \mathbf{b}_1, \\ \mathbf{W}'_l &= \mathbf{P}_{\tau_l}^\top \mathbf{W}_l \mathbf{P}_{\tau_{l-1}}, & \mathbf{b}'_l &= \mathbf{P}_{\tau_l}^\top \mathbf{b}_l, \quad l \in \{2, \dots, L-1\} \\ \mathbf{W}'_L &= \mathbf{W}_L \mathbf{P}_{\tau_{L-1}}, & \mathbf{b}'_L &= \mathbf{b}_L, \end{aligned}$$

where  $\mathbf{P}_{\tau_l} \in \{0, 1\}^{d_l \times d_l}$  is the permutation matrix corresponding to  $\tau_l \in S_{d_l}$  (see Figure 4 for an illustration). The action of  $G$  preserves the function represented by the network:  $\mathbf{f}_{g \cdot \theta} \equiv \mathbf{f}_\theta$ . Permutation symmetries naturally extend to many other neural architectures, see Kofinas et al. [41], Lim et al. [48], Zhou et al. [91] for a detailed discussion.

**Decomposed gradient symmetries.** Weight-space symmetries naturally extend to decomposed gradients. Following the discussion in Section 3, we define the decomposed gradient space of an MLP  $\mathbf{f}_\theta$  as

$$\Gamma := \Gamma^{(0)} \oplus \dots \oplus \Gamma^{(L)}, \quad (4)$$

where  $\Gamma^{(l)} := \mathbb{R}^{d_l \times 2}$ , referred to as the *neuron space* of the  $l$ -th layer, contains pairs  $\gamma^{(l)} = (\mathbf{a}^{(l)}, \mathbf{g}^{(l)})$  of activations and pre-activation gradients.  $\oplus$  denotes a direct sum of vector spaces.

$G$ ’s action extends naturally to  $\Gamma$ . For a decomposed gradient  $\gamma = (\gamma^{(0)}, \dots, \gamma^{(L)}) \in \Gamma$  and  $h = (\tau_1, \dots, \tau_{L-1}) \in G$ , the action  $h \cdot \gamma = (h \cdot \gamma^{(0)}, \dots, h \cdot \gamma^{(L)})$  is given by:

$$h \cdot \gamma^{(l)} = (\mathbf{P}_{\tau_l}^\top \mathbf{a}^{(l)}, \mathbf{P}_{\tau_l}^\top \mathbf{g}^{(l)}), \text{ for } l = 1, \dots, L-1, \quad h \cdot \gamma^{(l)} = \gamma^{(l)}, \text{ for } l = 1, L. \quad (5)$$

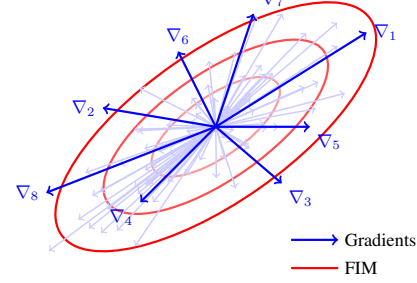


Figure 3: Fisher information as a second order approximation to the loss.

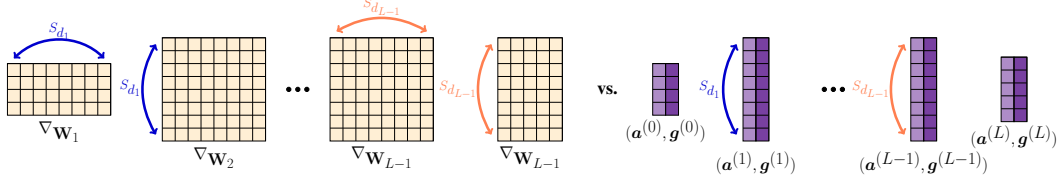


Figure 4: The action of  $G = S_{d_1} \times \dots \times S_{d_{L-1}}$  on parameter space performs simultaneous permutation of rows and columns of consecutive weight matrices. In contrast,  $G$ ’s action on the decomposed gradient space permutes the neuron space of each hidden layer independently.

Let  $\Phi_{(\mathbf{x}, \mathbf{y})} : \Theta \rightarrow \Gamma$  be the function that maps parameters  $\theta$  to the decomposition of the gradient  $\nabla_{(\mathbf{x}, \mathbf{y})} = \nabla_\theta \mathcal{L}_{(\mathbf{x}, \mathbf{y})}(\theta)$ .  $\Phi_{(\mathbf{x}, \mathbf{y})}$  is  $G$ -equivariant, that is:

$$\Phi_{(\mathbf{x}, \mathbf{y})}(h \cdot \theta) = h \cdot \Phi_{(\mathbf{x}, \mathbf{y})}(\theta). \quad (6)$$

This equivariance applies to any transformation that modifies or extracts information from the function represented by  $f_\theta$  using its gradients. As illustrated in Figure 4,  $G$ ’s action on  $\Gamma$  is simpler than its action on  $\Theta$ , since the permutations act independently on the different neuron spaces.

**Sets of decomposed gradients.** When computing the gradient of the loss over a batch  $\mathcal{B} \subseteq \mathcal{D}$ , we naturally obtain a set  $\{\nabla_{(\mathbf{x}, \mathbf{y})}\}_{(\mathbf{x}, \mathbf{y}) \in \mathcal{B}}$  of individual gradients<sup>2</sup>. As discussed in Section 3, this set contains implicit information about the local geometry of the loss landscape, which is critical for many tasks. Therefore, when designing methods for learning on gradients, it’s beneficial to process the entire collection rather than the gradient of the average loss. This intuition is formally motivated in Section 6.

As illustrated in Figure 2, gradients across a batch of size  $b$  can be efficiently represented as a tensor  $\mathbf{g} \in \Gamma_b$ , where the batched decomposed gradient space  $\Gamma_b$  is

$$\Gamma_b := \Gamma_b^{(0)} \oplus \dots \oplus \Gamma_b^{(L)}, \quad \Gamma_b^{(l)} := \mathbb{R}^{b \times d_l \times 2} \quad (7)$$

See formal definitions of all parameter and gradient spaces in Appendix C. Since the order of gradients in the batch is arbitrary, the set symmetry group is extended to  $G_b := S_b \times G$ . The action of  $(\tau, h) \in G_b$  permutes the batch indices using  $\tau$  and independently applies  $h$  across the neurons:

$$((\tau, h) \cdot \mathbf{g}^{(l)})_{j,:,:} = h \cdot \mathbf{g}_{\tau^{-1}(j),:,:}^{(l)}. \quad (8)$$

When modeling functions  $\Phi : \Gamma_b \rightarrow \Theta$ , we want to respect decomposed gradient symmetries ( $G$ -equivariance) and be independent of gradient ordering ( $S_b$ -invariance). We thus aim to design models that satisfy  $\Phi((\tau, h) \cdot \mathbf{g}) = h \cdot \Phi(\mathbf{g})$ .

**Extension to transformers.** The analysis above extends naturally to decomposed transformer gradients. The sequence dimension is treated as a batch dimension (with optional added sequence PE) and the neuron spaces correspond to the input and output of every linear layer and every query/key/value/output projection. Additionally, the neuron spaces across the residual stream are tied together having the same symmetry group. For a detailed discussion see Appendix B.2.

**Feature spaces.** As with other equivariant architectures, it is useful to extend  $\Gamma$  and  $\Gamma_b$  to more general feature spaces  $\Gamma_b[f]$  and  $\Gamma[f]$  by assigning an  $f$ -dimensional feature vector to each entry. See Appendix C for a formal definition.

## 5 GradMetaNet

In this section, we introduce GradMetaNet, an architecture for learning on gradients designed to process **sets of decomposed** gradients in a  $G_b$ -equivariant way. As the symmetry structure of  $\Gamma_b$  is simpler than that of  $\Theta_b$ , we can design GradMetaNet using simpler equivariant layers compared to its weight-space counterparts [61, 91, 92]. Specifically,  $\mathbf{g} \in \Gamma_b$  can be viewed as a set of decomposed gradients  $\{\gamma_1, \dots, \gamma_b\}$ , each of which is a concatenation of sets of neuron-level features  $\gamma_i = (\gamma_i^{(0)}, \dots, \gamma_i^{(L)})$ . To further simplify the symmetry structure, we incorporate a positional encoding map that enables us to treat each  $\gamma_i$  as a *single* bag of neuron-level features. This allows us to implement GradMetaNet using simple, well-established equivariant layers for sets [31, 67, 75, 90]. As illustrated in Figure 5, a GradMetaNet model  $\Phi$  is composed of a positional encoding map followed by a stack of equivariant linear layers of several types, interleaved with

<sup>2</sup>By “naturally” we mean that these gradients are always computed when backpropagating the average loss on the batch, and can be extracted using hooks *without additional cost*.

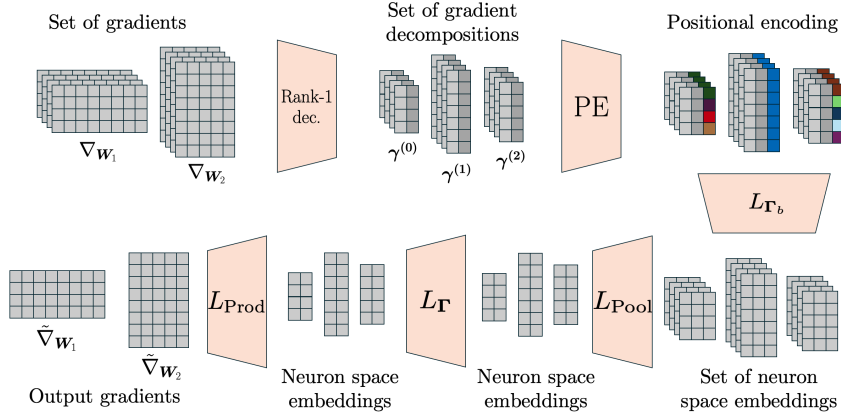


Figure 5: GradMetaNet pipeline: gradients are decomposed into rank-1 factors and positional encoding is applied. The input is then transformed by a stack of  $L_{\Gamma_b}$  equivariant interactions-across-sets layers.  $L_{\text{Pool}}$  pools these representations into  $\Gamma[f]$ , removing the batch dimension. Then a stack of  $L_{\Gamma}$  layers updates this representation, and  $L_{\text{Prod}}$  maps the result back to  $\Theta$ .

pointwise non-linearities.

$$\Phi = L_{\text{Prod}} \circ \sigma \circ L_{\Gamma}^{(k_2)} \circ \dots \circ \sigma \circ L_{\Gamma}^{(1)} \circ L_{\text{Pool}} \circ \sigma \circ L_{\Gamma_b}^{(k_1)} \circ \dots \circ \sigma \circ L_{\Gamma_b}^{(1)} \circ \text{PE}. \quad (9)$$

The following is a description of each layer:

- (I) Similarly to Lim et al. [48], Zhou et al. [92], we use a positional encoding map  $\text{PE} : \Gamma_b \rightarrow \Gamma_b[f]$  that concatenates a *layer identifier* each neurons in the intermediate layers and a *neuron identifier* to each neuron in the first and last layers. We use sinusoidal PE [79].
- (II)  $L_{\Gamma_b} : \Gamma_b[f_{\text{in}}] \rightarrow \Gamma_b[f_{\text{out}}]$  are then parametrized as the interactions-across-sets layers introduced in Hartford et al. [31] (batch dimension  $\times$  neuron dimension).
- (III) The pooling layer  $L_{\text{Pool}} : \Gamma_b[f_{\text{in}}] \rightarrow \Gamma[f_{\text{out}}]$  is designed to be  $S_b$ -invariant and  $G$ -equivariant, and is implemented as  $L_{\text{Pool}}(\mathbf{g}^{(l)})_{j,:} = M_1 \sum_{i'=1}^b \mathbf{g}_{i',j,:}^{(l)} + M_2 \sum_{l'=0}^L \sum_{i'=1}^b \sum_{j'=1}^{d_{i'}^{(l)}} \mathbf{g}_{i',j',,:}^{(l)}$ , for learnable  $M_1, M_2 \in \mathbb{R}^{f_{\text{out}} \times f_{\text{in}}}$ .
- (IV)  $L_{\Gamma} : \Gamma[f_{\text{in}}] \rightarrow \Gamma[f_{\text{out}}]$  are parameterized as equivariant DeepSets layers [90].
- (V) Finally, similarly to the generalized product layer in Navon et al. [61],  $L_{\text{Prod}} : \Gamma[f_{\text{in}}] \rightarrow \Theta$  applies a pointwise MLP to the features associated with the neurons connected to each weight:  $\mathbf{W}_{i,j}^{(l)} = \text{MLP}_1([\mathbf{g}_{i,:}^{(l)}, \mathbf{g}_{j,:}^{(l+1)}]), \mathbf{b}_i^{(l)} = \text{MLP}_2(\mathbf{g}_{i,:}^{(l)})$ .

For detailed descriptions and implementation details for all layers, a  $G$ -invariant head for invariant tasks, and other design choices see Appendix D.1.

**Extension to transformers.** As formally detailed and motivated in Appendix B, decomposed transformer gradients have an additional sequence dimension with a set symmetry structure and the neuron spaces across the residual stream are tied together. Therefore, when applying GradMetaNet, we treat the sequence dimension as the batch dimension (with optional sequence PE), stack all the neuron features across the residual stream together to a single neuron space, and extend our positional encoding to include the attention head indices. For an extended discussion see Appendix B.2 and B.3.

**GradMetaNet++.** Similarly to Kasten et al. [39], Lee et al. [46], Romero et al. [69], we can preserve equivariance by replacing summation in steps (II) and (VI) with attention mechanisms. Therefore, we introduce an attention-based variant of GradMetaNet, termed GradMetaNet++, where  $L_{\Gamma_b}$  and  $L_{\Gamma}$  are implemented using attention across the neuron and batch dimensions. This variant demonstrates significant performance improvements on some tasks, consistent with findings in previous studies. For a detailed description of GradMetaNet++ refer to Appendix D.2.

## 6 Theoretical Analysis

**Importance of processing sets of gradients.** Instead of processing the gradient of the average loss as in other gradient learning methods [18, 41, 91], GradMetaNet processes sets of (decomposed) gradients computed on individual datapoints. This approach is motivated by the fact that a set of

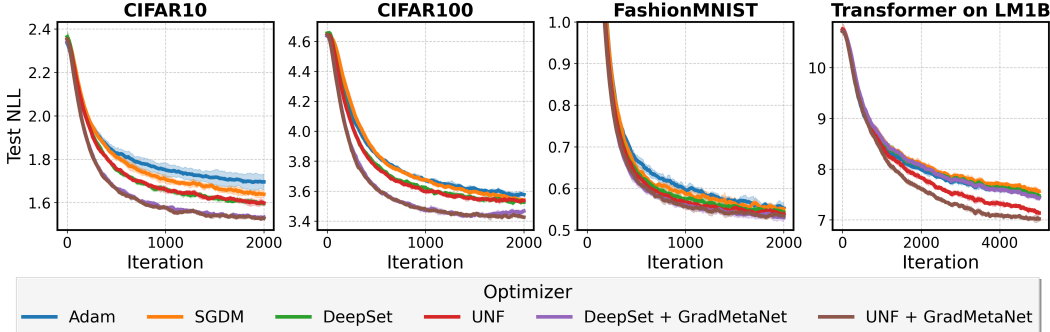


Figure 6: Test loss curves for MLP image classification tasks and a transformer language model trained on LM1B, using different optimizers and (learning rate tuned) Adam. Curves are smoothed and averaged over 5 random initializations, with shaded regions representing standard deviation.

gradients encodes strictly more information than the corresponding average gradient, enabling e.g. curvature estimations that cannot be computed using the average alone. This intuition is formalized in Appendix E.1, leading to Proposition 9 whose informal statement appears below.

**Proposition 1.** *Let  $\{\nabla_{(x,y)}\}_{(x,y) \in \mathcal{B}}$  be gradients computed on a set of datapoints  $\mathcal{B} \subseteq \mathcal{D}$ . There exist functions—such as natural gradient approximations or pruning saliency scores—that cannot be reconstructed from the average gradient  $\nabla_{\mathcal{B}}$  alone.*

**Expressive power.** Restricting a model to be equivariant with respect to a specific group action can potentially reduce its expressive power [51, 52, 59]. However, we demonstrate that GradMetaNet does not suffer from such limitations. Specifically, we prove a universal approximation property for equivariant functions defined on a compact domain that doesn’t intersect a certain low-dimensional subset  $\mathcal{E} \subset \Gamma_b$ . Formally:

**Theorem 2.** *Let  $\mathcal{K} \subset \Gamma_b$  be a compact domain such that  $\mathcal{K} = \cup_{g \in G_b} g \cdot \mathcal{K}$  and  $\mathcal{K} \cap \mathcal{E} = \emptyset$ . GradMetaNet models are universal approximators (in the  $\|\cdot\|_{\infty}$ -sense) of continuous  $G_b$ -equivariant functions from  $\mathcal{K}$  to  $\Theta$ .*

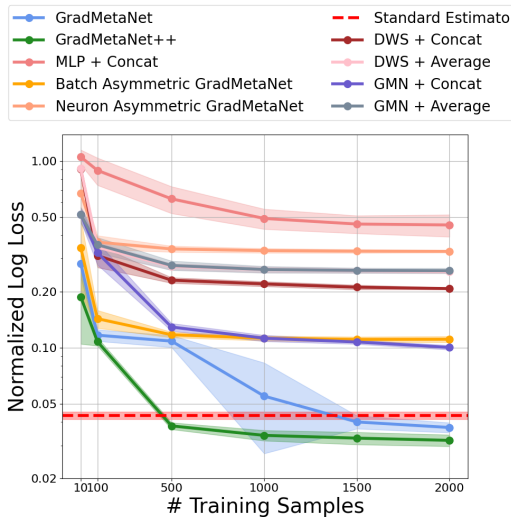


Figure 7: Comparison of gradient-learning models trained to predict the FIM diagonal from a sample of 128 gradients. Results are averaged over 5 seeds; shading represents standard deviation.

while retaining high expressive power, enabling it to represent all continuous functions on sets of gradients under mild assumptions.

$\mathcal{E}$  is the set of neuron features that have identical activations and backpropagated signals for at least two neurons (see Appendix E.2 for a precise definition). Similarly to Finkelshtain et al. [23], Maron et al. [53], the inclusion of  $\mathcal{E}$  in Theorem 2 is essential (see Appendix E.3). However,  $\mathcal{E}$  is a union of subspaces of co-dimension 2, has Lebesgue measure 0, and the conditions for membership in  $\mathcal{E}$  are highly unlikely in practice, making this assumption mild.

**Corollary 3.** *Let  $\mathcal{B}$  and  $\{\nabla_{(x,y)}\}_{(x,y) \in \mathcal{B}}$  be as in Proposition 1. Several natural functions—such as natural gradient approximations and pruning saliency scores—can be effectively approximated by GradMetaNet, which has access to  $\{\nabla_{(x,y)}\}_{(x,y) \in \mathcal{B}}$ , but cannot be approximated by methods that rely solely on  $\nabla_{\mathcal{B}}$ .*

For formal statements and proofs of all of the results in this section see Appendix E. In summary, GradMetaNet incorporates meaningful inductive biases for processing sets of gradients

## 7 Experiments

In this section, we evaluate GradMetaNet on a variety of learning tasks on gradients. We empirically demonstrate the importance of each of our design principles by ablating components and comparing to other baselines. We then showcase GradMetaNet’s effectiveness for three applications: curvature information estimation, learned optimization, and INR editing. Full experimental details appear in Appendix F.

### 7.1 Curvature Information Estimation

To demonstrate GradMetaNet’s ability to learn to approximate loss landscape curvature, we train it to predict the diagonal of the Fisher Information Matrix (FIM) from small samples of gradients. The diagonal of the FIM encodes the curvature along individual parameter directions, capturing the network’s sensitivity to a small change in each parameter.

**Data.** We first create a set of randomly initialized MLPs with 1-dimensional input and output. We then generate the targets by computing the FIM diagonal for each model over a sample of 1024 inputs in  $[-1, 1]$ . The input to each baseline is a smaller gradient sample computed over 128 points sampled from  $[-1, 1]$ .

**Baselines.** We compare GradMetaNet and GradMetaNet++ against a range of baselines, including architectures that (1) rely solely on the average gradient: DWS+Average [60], GMN+Average [41], (2) use full gradients instead of the rank-1 decomposition: DWS+Concat, GMN+Concat, or (3) (partially) disregard symmetries: Batch Asymmetric GradMetaNet, Neuron Asymmetric GradMetaNet, and MLP+Concat. See Appendix F.1 for full descriptions of the baselines.

**Results and discussion.** To measure the sample efficiency of each baseline, we repeat the experiment with a varying number of training examples (each training sample is still a set of 128 gradients, but we vary the *number of such sets* the models see during training). As seen in Figure 7, GradMetaNet and GradMetaNet++ perform significantly better than baselines across varying training set sizes. We also compare to a non-learnable approximation that directly estimates the diagonal of the FIM using the 128 input gradients (rather than the full set of 1024 datapoints). Only GradMetaNet and GradMetaNet++ outperform this baseline, achieving an improvement of 13.7% and 26.3% respectively. These results demonstrate GradMetaNet’s potential to learn more accurate approximations of gradient-based algorithms.

### 7.2 Learned Optimizers

Optimizing deep neural networks is one of the fundamental challenges of deep learning. While classical optimizers [19, 40, 62, 80] have become standard tools, their design largely relies on intuition and empirical validation. A promising alternative is to *learn* the optimization algorithm itself through meta-training [6, 8, 56]. Learned optimizers can potentially discover more effective update rules by adapting to the statistical patterns in loss landscapes. Most optimizers (learnable and hand-crafted) only process the averaged batch gradient, and therefore don’t have access to local curvature information. In this experiment we integrate GradMetaNet into learned optimizer architectures, providing it with the raw information required for computing the curvature in the form of sets of gradients on individual datapoints across batches.

Table 1: Multiplicative improvement in the number of steps to reach Adam’s best test loss. For each task, we run Adam, record its best test loss  $L$  and the number of steps  $N$  required to reach it. We then run standard and GradMetaNet-based learned optimizers, measure their steps to reach  $L$ , and report the improvement relative to  $N$ . Results are averaged over 5 runs. Full Results in Table 6.

Dataset	Optimizer	Avg. Step Reduction Factor vs. Adam ( $\uparrow$ )
F-MNIST	SGDM	1.13x
	DS	1.27x
	UNF	1.16x
	DS + GradMetaNet	1.44x
	UNF + GradMetaNet	<b>1.51x</b>
	SGDM	1.41x
CIFAR10	DS	2.32x
	UNF	2.64x
	DS + GradMetaNet	<b>4.63x</b>
	UNF + GradMetaNet	4.26x
	SGDM	1.06x
	DS	1.79x
CIFAR100	UNF	1.58x
	DS + GradMetaNet	<b>3.15x</b>
	UNF + GradMetaNet	2.85x
	SGDM	1.01x
	DS	0.88x
	UNF	1.48x
LM1B	DS + GradMetaNet	1.09x
	UNF + GradMetaNet	<b>1.82x</b>

**Setup.** Following Harrison et al. [30], Zhou et al. [91], we parametrize our learned optimizer rules as

$$\theta_{t+1} \leftarrow \theta_t + \alpha (\mathbf{v}_t^\mu + \beta \mathbf{F}_\phi(\theta_t, \nabla_t, \{\mathbf{v}_t^{\mu_i}\}_{i=1}^k)), \quad (10)$$

where  $\nabla_t$  is the current gradient, and  $\{\mathbf{v}_t^{\mu_i}\}_{i=1}^k$  are momentum terms with different decay rates. The standard architecture for  $\mathbf{F}_\phi$  is DeepSets (DS) [90] which applies a per-parameter MLP to the input features. More recently, researchers have explored using equivariant weight-space architectures like Universal Neural Functionals (UNF) [91] to implement  $\mathbf{F}_\phi$ . For GradMetaNet-based learned optimizers we parametrize  $\mathbf{F}_\phi$  as

$$\mathbf{F}_\phi(\theta_t, \nabla_t, \{\mathbf{v}_t^{\mu_i}\}_{i=1}^k, t, \mathbf{F}_\psi^{\text{GradMetaNet}}(\mathbf{g}_t, \{\mathbf{v}_t^{\mu_i}\}_{i=1}^k)), \quad (11)$$

where  $\mathbf{g}_t \in \Gamma_b$  is the set of decomposed gradients across the current batch, and  $\{\mathbf{v}_t^{\mu_i}\}_i$  are exponential moving averages of past  $\mathbf{g}_t$ s with different decay rates. The learnable meta-parameters  $\alpha, \beta, \mu, \phi$ , and  $\psi$  are optimized during meta-training (using PES [84]) to minimize the training loss after  $T$  steps. We evaluate five types of architectures: DeepSets, UNF, DeepSets + GradMetaNet, UNF + GradMetaNet, and learnable SGD with momentum (taking  $\beta = 0$  in Equation 10).

**Tasks.** We use three types of optimization tasks: (1) optimizing a 2-parameter linear regression, constructed to have non-diagonal curvature, (2) optimizing MLPs for classifying CIFAR10, CIFAR100 [44], and FashionMNIST [89] images, and (3) optimizing transformer based language models on LM1B [14]. For a detailed description of each task and the meta-training setup see Appendix F.2.

**Results and discussion.** As Figure 8 demonstrates, for the 2-parameter regressions task, GradMetaNet-based learned optimizers can use the curvature of the loss landscape to avoid redundant steps. Consequently, as seen in Table 1 and Figure 6, GradMetaNet-based learned optimizers consistently outperform baselines across optimization tasks for both MLP and transformers.

### 7.3 INR Editing

Implicit Neural Representations (INRs) [63, 77] use neural networks to encode images as functions. In this experiment, we explore the task of INR editing, where the goal is to adapt the weights of an INR to modify the image it represents. This involves directly adjusting the INR’s parameters by learning a metanetwork predicting a parameter delta  $\Delta\theta$ , and updating the model with  $\theta' = \theta + \Delta\theta$ .

**Data.** Following previous works [38, 92, 93], we use two standard benchmarks: figure dilation for MNIST INRs and contrast enhancement for CIFAR-10 INRs. For each INR, we compute the parameter gradients with respect to the MSE loss between the INR output and the target edited image, evaluated over randomly sampled points. The input data consists of both the parameters of the INR and the corresponding gradients.

**Baselines.** We evaluate GradMetaNet and GradMetaNet++ in combination with several weight-space architectures. GradMetaNet and GradMetaNet++ process the gradients to produce outputs in  $\Theta$ , which are then used as additional weight features for the base weight-space network. This hybrid approach is compared against two baselines: (1) the base weight-space network, and (2) the base weight-space network augmented with probing features. Following Kofinas et al. [41], the probing features are activations evaluated at randomly sampled grid points, incorporated as additional bias features.

**Results and Discussion.** As seen in Table 2, both GradMetaNet and GradMetaNet++ consistently improve the performance of weight-space models, achieve greater performance gains than probing, and improve the current state-of-the-art for weight-space model editing.

## 8 Conclusion and Limitations

**Conclusion.** We introduce GradMetaNet, an equivariant architecture for processing sets of decomposed gradients, supported by both theoretical and experimental results. Theoretically, we demonstrate that under mild assumptions GradMetaNet can approximate any function processing sets of gradients, and that average gradient methods are unable to approximate several natural gradient-based functions. Experimentally, we demonstrate GradMetaNet’s ability to predict local curvature, enhance learned optimizers, and achieve state-of-the-art performance in model editing.

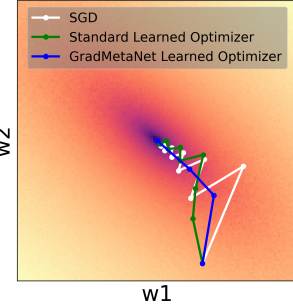


Figure 8: GradMetaNet-based learned optimizers can account for loss-landscape curvature, avoiding redundant steps.

Table 2: INR editing results on MNIST (dilation) and CIFAR10 (contrast). MSE ( $\downarrow$ ) is reported in  $10^{-2}$  for MNIST and  $10^{-3}$  for CIFAR10. Results are averaged over 3 seeds.

	MNIST			CIFAR10		
	DWS [60]	GMN [41]	ScaleGMN [38]	DWS [60]	GMN [41]	ScaleGMN [38]
WS	$2.29 \pm 0.01$	$1.96 \pm 0.02$	$1.99 \pm 0.02$	$5.57 \pm 0.02$	$5.09 \pm 0.05$	$5.23 \pm 0.13$
WS + Probing	$2.36 \pm 0.06$	$1.85 \pm 0.00$	$1.92 \pm 0.04$	$4.22 \pm 0.08$	$3.81 \pm 0.02$	$3.87 \pm 0.05$
WS + GradMetaNet	$2.28 \pm 0.02$	<b><math>1.70 \pm 0.01</math></b>	$1.70 \pm 0.00$	$4.10 \pm 0.10$	$3.65 \pm 0.01$	$3.69 \pm 0.09$
WS + GradMetaNet++	<b><math>1.95 \pm 0.01</math></b>	$1.71 \pm 0.00$	<b><math>1.60 \pm 0.00</math></b>	<b><math>3.86 \pm 0.02</math></b>	<b><math>2.99 \pm 0.03</math></b>	<b><math>3.00 \pm 0.00</math></b>

**Limitations and future work.** The current implementation of GradMetaNet is limited to MLPs and transformers, in future work we hope to extend GradMetaNet to support other neural architectures. Additionally, GradMetaNet++’s use of attention mechanisms limits its usage in large-scale settings. Finally, scaling GradMetaNet, GradMetaNet++ or their variants to larger models, such as state-of-the-art LLMs and generative models, is an interesting direction for future work.

## Acknowledgments

YG is supported by the the UKRI Engineering and Physical Sciences Research Council (EPSRC) CDT in Autonomous and Intelligent Machines and Systems (grant reference EP/S024050/1). MB is supported by EPSRC Turing AI World-Leading Research Fellowship No. EP/X040062/1 and EPSRC AI Hub on Mathematical Foundations of Intelligence: An “Erlangen Programme” for AI No. EP/Y028872/1. HM is a he Robert J. Shillman Fellow, and is supported by the Israel Science Foundation through a personal grant (ISF 264/23) and an equipment grant (ISF 532/23).

## References

- [1] Samuel K Ainsworth, Jonathan Hayase, and Siddhartha Srinivasa. Git re-basin: Merging models modulo permutation symmetries. *arXiv preprint arXiv:2209.04836*, 2022.
- [2] Marjan Albooyeh, Daniele Bertolini, and Siamak Ravanbakhsh. Incidence networks for geometric deep learning. *arXiv preprint arXiv:1905.11460*, 2019.
- [3] Shun-Ichi Amari. Natural gradient works efficiently in learning. *Neural computation*, 10(2):251–276, 1998.
- [4] Shun-ichi Amari and Hiroshi Nagaoka. *Methods of information geometry*, volume 191. American Mathematical Soc., 2000.
- [5] Bruno Andreis, Soro Bedionita, and Sung Ju Hwang. Set-based neural network encoding. *arXiv preprint arXiv:2305.16625*, 2023.
- [6] Marcin Andrychowicz, Misha Denil, Sergio Gomez, Matthew W Hoffman, David Pfau, Tom Schaul, Brendan Shillingford, and Nando De Freitas. Learning to learn by gradient descent by gradient descent. *Advances in neural information processing systems*, 29, 2016.
- [7] Erik J Bekkers. B-spline cnns on lie groups. *arXiv preprint arXiv:1909.12057*, 2019.
- [8] Yoshua Bengio, Samy Bengio, and Jocelyn Cloutier. *Learning a synaptic learning rule*. Citeseer, 1990.
- [9] Léon Bottou. Large-scale machine learning with stochastic gradient descent. In *Proceedings of COMPSTAT’2010: 19th International Conference on Computational StatisticsParis France, August 22-27, 2010 Keynote, Invited and Contributed Papers*, pages 177–186. Springer, 2010.
- [10] G. Bradski. The OpenCV Library. *Dr. Dobb’s Journal of Software Tools*, 2000.
- [11] Johann Brehmer, Sönke Behrends, Pim de Haan, and Taco Cohen. Does equivariance matter at scale? *arXiv preprint arXiv:2410.23179*, 2024.
- [12] Michael M Bronstein, Joan Bruna, Yann LeCun, Arthur Szlam, and Pierre Vandergheynst. Geometric deep learning: going beyond euclidean data. *IEEE Signal Processing Magazine*, 34(4):18–42, 2017.

- [13] Michael M Bronstein, Joan Bruna, Taco Cohen, and Petar Veličković. Geometric deep learning: Grids, groups, graphs, geodesics, and gauges. *arXiv preprint arXiv:2104.13478*, 2021.
- [14] Ciprian Chelba, Tomas Mikolov, Mike Schuster, Qi Ge, Thorsten Brants, Philipp Koehn, and Tony Robinson. One billion word benchmark for measuring progress in statistical language modeling. *arXiv preprint arXiv:1312.3005*, 2013.
- [15] Taco Cohen and Max Welling. Group equivariant convolutional networks. In *International conference on machine learning*, pages 2990–2999. PMLR, 2016.
- [16] Taco Cohen et al. *Equivariant convolutional networks*. PhD thesis, Taco Cohen, 2021.
- [17] Erik Daxberger, Agustinus Kristiadi, Alexander Immer, Runa Eschenhagen, Matthias Bauer, and Philipp Hennig. Laplace redux-effortless bayesian deep learning. *Advances in Neural Information Processing Systems*, 34:20089–20103, 2021.
- [18] Nicola De Cao, Wilker Aziz, and Ivan Titov. Editing factual knowledge in language models. *arXiv preprint arXiv:2104.08164*, 2021.
- [19] John Duchi, Elad Hazan, and Yoram Singer. Adaptive subgradient methods for online learning and stochastic optimization. *Journal of machine learning research*, 12(7), 2011.
- [20] Gabriel Eilertsen, Daniel Jönsson, Timo Ropinski, Jonas Unger, and Anders Ynnerman. Classifying the classifier: dissecting the weight space of neural networks. In *ECAI 2020*, pages 1119–1126. IOS Press, 2020.
- [21] Runa Eschenhagen, Alexander Immer, Richard Turner, Frank Schneider, and Philipp Hennig. Kronecker-factored approximate curvature for modern neural network architectures. *Advances in Neural Information Processing Systems*, 36:33624–33655, 2023.
- [22] Carlos Esteves, Christine Allen-Blanchette, Ameesh Makadia, and Kostas Daniilidis. Learning so (3) equivariant representations with spherical cnns. In *Proceedings of the European Conference on Computer Vision (ECCV)*, pages 52–68, 2018.
- [23] Ben Finkelshtein, İsmail İlkan Ceylan, Michael Bronstein, and Ron Levie. Equivariance everywhere all at once: A recipe for graph foundation models. *arXiv preprint arXiv:2506.14291*, 2025.
- [24] Marc Finzi, Samuel Stanton, Pavel Izmailov, and Andrew Gordon Wilson. Generalizing convolutional neural networks for equivariance to lie groups on arbitrary continuous data. In *International Conference on Machine Learning*, pages 3165–3176. PMLR, 2020.
- [25] Thomas George, César Laurent, Xavier Bouthillier, Nicolas Ballas, and Pascal Vincent. Fast approximate natural gradient descent in a kronecker factored eigenbasis. *Advances in Neural Information Processing Systems*, 31, 2018.
- [26] Thomas George, César Laurent, Xavier Bouthillier, Nicolas Ballas, and Pascal Vincent. Fast approximate natural gradient descent in a kronecker factored eigenbasis. *Advances in Neural Information Processing Systems*, 31, 2018.
- [27] Roger Grosse and James Martens. A kronecker-factored approximate fisher matrix for convolution layers. In *International Conference on Machine Learning*, pages 573–582. PMLR, 2016.
- [28] Roger Grosse, Juhan Bae, Cem Anil, Nelson Elhage, Alex Tamkin, Amirhossein Tajdini, Benoit Steiner, Dustin Li, Esin Durmus, Ethan Perez, et al. Studying large language model generalization with influence functions. *arXiv preprint arXiv:2308.03296*, 2023.
- [29] Vineet Gupta, Tomer Koren, and Yoram Singer. Shampoo: Preconditioned stochastic tensor optimization. In *International Conference on Machine Learning*, pages 1842–1850. PMLR, 2018.
- [30] James Harrison, Luke Metz, and Jascha Sohl-Dickstein. A closer look at learned optimization: Stability, robustness, and inductive biases. *Advances in Neural Information Processing Systems*, 35:3758–3773, 2022.

[31] Jason Hartford, Devon Graham, Kevin Leyton-Brown, and Siamak Ravanbakhsh. Deep models of interactions across sets. In *International Conference on Machine Learning*, pages 1909–1918. PMLR, 2018.

[32] Babak Hassibi, David G Stork, and Gregory J Wolff. Optimal brain surgeon and general network pruning. In *IEEE international conference on neural networks*, pages 293–299. IEEE, 1993.

[33] Robert Hecht-Nielsen. On the algebraic structure of feedforward network weight spaces. In *Advanced Neural Computers*, pages 129–135. Elsevier, 1990.

[34] Vincent Herrmann, Francesco Faccio, and Jürgen Schmidhuber. Learning useful representations of recurrent neural network weight matrices. *arXiv preprint arXiv:2403.11998*, 2024.

[35] Eliahu Horwitz, Bar Cavia, Jonathan Kahana, and Yedid Hoshen. Representing model weights with language using tree experts. *arXiv preprint arXiv:2410.13569*, 2024.

[36] Alexander Immer, Matthias Bauer, Vincent Fortuin, Gunnar Rätsch, and Khan Mohammad Emamiyaz. Scalable marginal likelihood estimation for model selection in deep learning. In *International Conference on Machine Learning*, pages 4563–4573. PMLR, 2021.

[37] Jonathan Kahana, Eliahu Horwitz, Imri Shuval, and Yedid Hoshen. Deep linear probe generators for weight space learning. *arXiv preprint arXiv:2410.10811*, 2024.

[38] Ioannis Kalogeropoulos, Giorgos Bouritsas, and Yannis Panagakis. Scale equivariant graph metanetworks. *arXiv preprint arXiv:2406.10685*, 2024.

[39] Yoni Kasten, Wuyue Lu, and Haggai Maron. Fast encoder-based 3d from casual videos via point track processing. In *The Thirty-eighth Annual Conference on Neural Information Processing Systems*, 2024.

[40] Diederik P Kingma. Adam: A method for stochastic optimization. *arXiv preprint arXiv:1412.6980*, 2014.

[41] Miltiadis Kofinas, Boris Knyazev, Yan Zhang, Yunlu Chen, Gertjan J Burghouts, Efstratios Gavves, Cees GM Snoek, and David W Zhang. Graph neural networks for learning equivariant representations of neural networks. *arXiv preprint arXiv:2403.12143*, 2024.

[42] Pang Wei Koh and Percy Liang. Understanding black-box predictions via influence functions. In *International conference on machine learning*, pages 1885–1894. PMLR, 2017.

[43] Risi Kondor and Shubhendu Trivedi. On the generalization of equivariance and convolution in neural networks to the action of compact groups. In *International conference on machine learning*, pages 2747–2755. PMLR, 2018.

[44] Alex Krizhevsky, Geoffrey Hinton, et al. Learning multiple layers of features from tiny images. Technical Report 4, University of Toronto, 2009.

[45] Yann LeCun, John Denker, and Sara Solla. Optimal brain damage. *Advances in neural information processing systems*, 2, 1989.

[46] Juho Lee, Yoonho Lee, Jungtaek Kim, Adam Kosiorek, Seungjin Choi, and Yee Whye Teh. Set transformer: A framework for attention-based permutation-invariant neural networks. In *International conference on machine learning*, pages 3744–3753. PMLR, 2019.

[47] Derek Lim, Joshua Robinson, Lingxiao Zhao, Tess Smidt, Suvrit Sra, Haggai Maron, and Stefanie Jegelka. Sign and basis invariant networks for spectral graph representation learning. *arXiv preprint arXiv:2202.13013*, 2022.

[48] Derek Lim, Haggai Maron, Marc T Law, Jonathan Lorraine, and James Lucas. Graph metanetworks for processing diverse neural architectures. *arXiv preprint arXiv:2312.04501*, 2023.

[49] Jingyuan Liu, Jianlin Su, Xingcheng Yao, Zhejun Jiang, Guokun Lai, Yulun Du, Yidao Qin, Weixin Xu, Enzhe Lu, Junjie Yan, et al. Muon is scalable for llm training. *arXiv preprint arXiv:2502.16982*, 2025.

[50] Ilya Loshchilov and Frank Hutter. Decoupled weight decay regularization. In *International Conference on Learning Representations*, 2019. URL <https://openreview.net/forum?id=Bkg6RiCqY7>.

[51] Haggai Maron, Heli Ben-Hamu, Hadar Serviansky, and Yaron Lipman. Provably powerful graph networks. *Advances in neural information processing systems*, 32, 2019.

[52] Haggai Maron, Ethan Fetaya, Nimrod Segol, and Yaron Lipman. On the universality of invariant networks. In *International conference on machine learning*, pages 4363–4371. PMLR, 2019.

[53] Haggai Maron, Or Litany, Gal Chechik, and Ethan Fetaya. On learning sets of symmetric elements. In *International conference on machine learning*, pages 6734–6744. PMLR, 2020.

[54] James Martens. New insights and perspectives on the natural gradient method. *Journal of Machine Learning Research*, 21(146):1–76, 2020.

[55] James Martens and Roger Grosse. Optimizing neural networks with kronecker-factored approximate curvature. In *International conference on machine learning*, pages 2408–2417. PMLR, 2015.

[56] Luke Metz, Niru Maheswaranathan, Jeremy Nixon, Daniel Freeman, and Jascha Sohl-Dickstein. Understanding and correcting pathologies in the training of learned optimizers. In *International Conference on Machine Learning*, pages 4556–4565. PMLR, 2019.

[57] Luke Metz, C Daniel Freeman, James Harrison, Niru Maheswaranathan, and Jascha Sohl-Dickstein. Practical tradeoffs between memory, compute, and performance in learned optimizers. In *Conference on Lifelong Learning Agents (CoLLAs)*, 2022. URL [http://github.com/google/learned\\_optimization](http://github.com/google/learned_optimization).

[58] Eric Mitchell, Charles Lin, Antoine Bosselut, Chelsea Finn, and Christopher D Manning. Fast model editing at scale. *arXiv preprint arXiv:2110.11309*, 2021.

[59] Christopher Morris, Martin Ritzert, Matthias Fey, William L Hamilton, Jan Eric Lenssen, Gaurav Rattan, and Martin Grohe. Weisfeiler and leman go neural: Higher-order graph neural networks. In *Proceedings of the AAAI conference on artificial intelligence*, volume 33, pages 4602–4609, 2019.

[60] Aviv Navon, Aviv Shamsian, Idan Achituve, Ethan Fetaya, Gal Chechik, and Haggai Maron. Equivariant architectures for learning in deep weight spaces. In *International Conference on Machine Learning*, pages 25790–25816. PMLR, 2023.

[61] Aviv Navon, Aviv Shamsian, Ethan Fetaya, Gal Chechik, Nadav Dym, and Haggai Maron. Equivariant deep weight space alignment. *arXiv preprint arXiv:2310.13397*, 2023.

[62] Yurii Nesterov. A method for unconstrained convex minimization problem with the rate of convergence  $o(1/k^2)$ . In *Dokl. Akad. Nauk. SSSR*, volume 269, page 543, 1983.

[63] Jeong Joon Park, Peter Florence, Julian Straub, Richard Newcombe, and Steven Lovegrove. Deepsdf: Learning continuous signed distance functions for shape representation. In *Proceedings of the IEEE/CVF conference on computer vision and pattern recognition*, pages 165–174, 2019.

[64] R Pascanu. Revisiting natural gradient for deep networks. *arXiv preprint arXiv:1301.3584*, 2013.

[65] Adam Paszke, Sam Gross, Francisco Massa, Adam Lerer, James Bradbury, Gregory Chanan, Trevor Killeen, Zeming Lin, Natalia Gimelshein, Luca Antiga, et al. Pytorch: An imperative style, high-performance deep learning library. *Advances in neural information processing systems*, 32, 2019.

[66] William Peebles, Ilija Radosavovic, Tim Brooks, Alexei A Efros, and Jitendra Malik. Learning to learn with generative models of neural network checkpoints. *arXiv preprint arXiv:2209.12892*, 2022.

[67] Charles R Qi, Hao Su, Kaichun Mo, and Leonidas J Guibas. Pointnet: Deep learning on point sets for 3d classification and segmentation. In *Proceedings of the IEEE conference on computer vision and pattern recognition*, pages 652–660, 2017.

[68] Siamak Ravanbakhsh, Jeff Schneider, and Barnabas Poczos. Equivariance through parameter-sharing. In *International conference on machine learning*, pages 2892–2901. PMLR, 2017.

[69] David Romero, Erik Bekkers, Jakub Tomczak, and Mark Hoogendoorn. Attentive group equivariant convolutional networks. In *International Conference on Machine Learning*, pages 8188–8199. PMLR, 2020.

[70] David E Rumelhart, Geoffrey E Hinton, and Ronald J Williams. Learning representations by back-propagating errors. *nature*, 323(6088):533–536, 1986.

[71] Victor Garcia Satorras, Emiel Hoogeboom, and Max Welling. E (n) equivariant graph neural networks. In *International conference on machine learning*, pages 9323–9332. PMLR, 2021.

[72] Konstantin Schürholt, Dimche Kostadinov, and Damian Borth. Self-supervised representation learning on neural network weights for model characteristic prediction. *Advances in Neural Information Processing Systems*, 34:16481–16493, 2021.

[73] Konstantin Schürholt, Boris Knyazev, Xavier Giró-i Nieto, and Damian Borth. Hyper-representations as generative models: Sampling unseen neural network weights. *Advances in Neural Information Processing Systems*, 35:27906–27920, 2022.

[74] Konstantin Schürholt, Michael W Mahoney, and Damian Borth. Towards scalable and versatile weight space learning. *arXiv preprint arXiv:2406.09997*, 2024.

[75] Hadar Serviansky, Nimrod Segol, Jonathan Shlomi, Kyle Cranmer, Eilam Gross, Haggai Maron, and Yaron Lipman. Set2graph: Learning graphs from sets. *Advances in Neural Information Processing Systems*, 33:22080–22091, 2020.

[76] Berfin Simsek, Johann Brea, Bernd Illing, and Wulfram Gerstner. Weight-space symmetry in neural network loss landscapes revisited. 2020.

[77] Vincent Sitzmann, Julien Martel, Alexander Bergman, David Lindell, and Gordon Wetzstein. Implicit neural representations with periodic activation functions. *Advances in neural information processing systems*, 33:7462–7473, 2020.

[78] Behrooz Tahmasebi and Stefanie Jegelka. The exact sample complexity gain from invariances for kernel regression. *Advances in Neural Information Processing Systems*, 36, 2023.

[79] Matthew Tancik, Pratul Srinivasan, Ben Mildenhall, Sara Fridovich-Keil, Nithin Raghavan, Utkarsh Singhal, Ravi Ramamoorthi, Jonathan Barron, and Ren Ng. Fourier features let networks learn high frequency functions in low dimensional domains. *Advances in neural information processing systems*, 33:7537–7547, 2020.

[80] Tijmen Tieleman. Lecture 6.5-rmsprop: Divide the gradient by a running average of its recent magnitude. *COURSERA: Neural networks for machine learning*, 4(2):26, 2012.

[81] Thomas Unterthiner, Daniel Keysers, Sylvain Gelly, Olivier Bousquet, and Ilya Tolstikhin. Predicting neural network accuracy from weights. *arXiv preprint arXiv:2002.11448*, 2020.

[82] Tycho FA van der Ouderaa, Markus Nagel, Mart Van Baalen, Yuki M Asano, and Tijmen Blankevoort. The llm surgeon. *arXiv preprint arXiv:2312.17244*, 2023.

[83] Ashish Vaswani, Noam Shazeer, Niki Parmar, Jakob Uszkoreit, Llion Jones, Aidan N Gomez, Łukasz Kaiser, and Illia Polosukhin. Attention is all you need. *Advances in neural information processing systems*, 30, 2017.

[84] Paul Vicol, Luke Metz, and Jascha Sohl-Dickstein. Unbiased gradient estimation in unrolled computation graphs with persistent evolution strategies. In *International Conference on Machine Learning*, pages 10553–10563. PMLR, 2021.

[85] Nikhil Vyas, Depen Morwani, Rosie Zhao, Mujin Kwun, Itai Shapira, David Brandfonbrener, Lucas Janson, and Sham Kakade. Soap: Improving and stabilizing shampoo using adam. *arXiv preprint arXiv:2409.11321*, 2024.

[86] Edward Wagstaff, Fabian B Fuchs, Martin Engelcke, Michael A Osborne, and Ingmar Posner. Universal approximation of functions on sets. *Journal of Machine Learning Research*, 23(151):1–56, 2022.

[87] Chaoqi Wang, Roger Grosse, Sanja Fidler, and Guodong Zhang. Eigendamage: Structured pruning in the kronecker-factored eigenbasis. In *International conference on machine learning*, pages 6566–6575. PMLR, 2019.

[88] Boris Weisfeiler and Andrei Leman. The reduction of a graph to canonical form and the algebra which appears therein. *nti, Series*, 2(9):12–16, 1968.

[89] Han Xiao, Kashif Rasul, and Roland Vollgraf. Fashion-mnist: a novel image dataset for benchmarking machine learning algorithms. *arXiv preprint arXiv:1708.07747*, 2017.

[90] Manzil Zaheer, Satwik Kottur, Siamak Ravanbakhsh, Barnabas Poczos, Russ R Salakhutdinov, and Alexander J Smola. Deep sets. *Advances in neural information processing systems*, 30, 2017.

[91] Allan Zhou, Chelsea Finn, and James Harrison. Universal neural functionals. *arXiv preprint arXiv:2402.05232*, 2024.

[92] Allan Zhou, Kaien Yang, Kaylee Burns, Adriano Cardace, Yiding Jiang, Samuel Sokota, J Zico Kolter, and Chelsea Finn. Permutation equivariant neural functionals. *Advances in neural information processing systems*, 36, 2024.

[93] Allan Zhou, Kaien Yang, Yiding Jiang, Kaylee Burns, Winnie Xu, Samuel Sokota, J Zico Kolter, and Chelsea Finn. Neural functional transformers. *Advances in neural information processing systems*, 36, 2024.

## A Extended Background

### A.1 Gradient Decomposition for MLPs

Using the notation introduced in Section 3, for  $l = 1, \dots, L$ ,  $n = 1, \dots, d_{l-1}$ ,  $m = 1, \dots, d_l$  we apply the chain rule to get

$$(\nabla_{\mathbf{W}_l} \mathcal{L}_{(\mathbf{x}, \mathbf{y})}(\boldsymbol{\theta}))_{n,m} = \sum_{k=1}^{d_l} \left( \frac{\partial \mathcal{L}_{(\mathbf{x}, \mathbf{y})}(\boldsymbol{\theta})}{\partial (\mathbf{u}^{(l)})_k} \right) \cdot \left( \frac{\partial (\mathbf{u}^{(l)})_k}{\partial (\mathbf{W}_l)_{n,m}} \right) = \sum_{k=1}^{d_l} (\mathbf{g}^{(l)})_k (\delta_{n,k} (\mathbf{a}^{(l-1)})_n) = (\mathbf{g}^{(l)})_m (\mathbf{a}^{(l-1)})_n, \quad (12)$$

where  $\delta_{n,k}$  is the Dirac delta defined by  $\delta_{n,k} = \begin{cases} 1 & n = k \\ 0 & n \neq k. \end{cases}$  Similarly

$$(\nabla_{\mathbf{b}_l} \mathcal{L}_{(\mathbf{x}, \mathbf{y})}(\boldsymbol{\theta}))_m = \sum_{k=1}^{d_l} \left( \frac{\partial \mathcal{L}_{(\mathbf{x}, \mathbf{y})}(\boldsymbol{\theta})}{\partial (\mathbf{u}^{(l)})_k} \right) \cdot \left( \frac{\partial (\mathbf{u}^{(l)})_k}{\partial (\mathbf{b}_l)_m} \right) = \sum_{k=1}^{d_l} (\mathbf{g}^{(l)})_k \delta_{m,k} = (\mathbf{g}^{(l)})_m. \quad (13)$$

Therefore,

$$\nabla_{\mathbf{W}_l} \mathcal{L}_{(\mathbf{x}, \mathbf{y})}(\boldsymbol{\theta}) = \mathbf{g}^{(l)} (\mathbf{a}^{(l-1)})^\top, \quad \nabla_{\mathbf{b}_l} \mathcal{L}_{(\mathbf{x}, \mathbf{y})}(\boldsymbol{\theta}) = \mathbf{g}^{(l)} \quad (14)$$

as discussed in Section 3.

### A.2 Extracting Activations and Pre-Activation Gradient Signals

As mentioned in Section 3 the activations ( $\mathbf{a}^{(l)}$ ) and pre-activation gradient signals ( $\mathbf{g}^{(l)}$ ) used for the gradient decomposition are naturally computed during backpropagation and don't need to be recomputed. The following is a PyTorch code example for extracting these components without additional cost using forward/backward hooks:

```

import torch
import torch.nn as nn
import torch.nn.functional as F

class MLP(nn.Module):
    def __init__(self):
        super(MLP, self).__init__()
        self.fc1 = nn.Linear(8, 32)
        self.fc2 = nn.Linear(32, 16)
        self.fc3 = nn.Linear(16, 3)

    def forward(self, x):
        x = F.relu(self.fc1(x))
        x = F.relu(self.fc2(x))
        x = self.fc3(x)
        return x

activations = []
tangents = []

def forward_hook(module, inp, out):
    activations[module] = inp[0].detach()

def backward_hook(module, grad_inp, grad_out):
    tangents[module] = grad_out[0].detach()

model = MLP()

# Set hooks
model.fc1.register_forward_hook(forward_hook)
model.fc1.register_full_backward_hook(backward_hook)
model.fc2.register_forward_hook(forward_hook)
model.fc2.register_full_backward_hook(backward_hook)
model.fc3.register_forward_hook(forward_hook)
model.fc3.register_full_backward_hook(backward_hook)

# Backpropagate loss
x = torch.randn(4, 8) # (batch, input)
target = torch.randn(4, 3) # (batch, input)
output = model(x)
loss = F.mse_loss(output, target)
loss.backward()

print(activations)
print(tangents)

```

### A.3 The Fisher Information Matrix and Its Uses

Many gradient-based algorithms [17, 27, 55, 82, 87] use the Fisher Information Matrix (FIM) to approximate the curvature of the loss landscape. Below, we define the FIM and present two common gradient-based algorithms that utilize it. The FIM has numerous other applications, this section serves only as a basic introduction. For a more comprehensive overview, we refer readers to [54, 64].

**The Fisher information matrix.** Consider a supervised learning problem of predicting outputs  $\mathbf{y} \in \mathcal{Y}$  from inputs  $\mathbf{x} \in \mathcal{X}$ . We assume a probabilistic model of the form  $p_{\theta}(\mathbf{y}|\mathbf{x}) = p(\mathbf{y}|\mathbf{f}_{\theta}(\mathbf{x}))$ , where  $p$  is called the *likelihood*. For classification tasks we may assume a softmax likelihood,  $p(\mathbf{y} = k|\mathbf{f}_{\theta}(\mathbf{x})) = \text{softmax}(\mathbf{f}_{\theta}(\mathbf{x}))_k$ , and for regression, we usually take a Gaussian likelihood  $p(\mathbf{y}|\mathbf{f}_{\theta}(\mathbf{x})) = \mathcal{N}(\mathbf{y}; \mathbf{f}_{\theta}(\mathbf{x}), \mathbf{I})$ .  $p_{\theta}(\mathbf{y}|\mathbf{x})$  is called the *predictive distribution*. The FIM is defined by

$$\mathbf{F} = \mathbb{E}_{\mathbf{x} \sim \mathcal{D}, \mathbf{y} \sim p_{\theta}(\mathbf{y}|\mathbf{x})} (\nabla_{\theta} \log(p_{\theta}(\mathbf{y}|\mathbf{x})) \nabla_{\theta} \log(p_{\theta}(\mathbf{y}|\mathbf{x})))^\top \in \Theta \otimes \Theta \quad (15)$$

The FIM is a second order approximation of the change in the model's predictive distribution with respect to the parameters

$$\mathbb{E}_{\mathbf{x} \sim \mathcal{D}} (D_{\text{KL}} (p_{\boldsymbol{\theta}}(\mathbf{y}|\mathbf{x}) \parallel p_{\boldsymbol{\theta}+\boldsymbol{\delta}}(\mathbf{y}|\mathbf{x}))) = \frac{1}{2} \boldsymbol{\delta}^\top \mathbf{F} \boldsymbol{\delta} + \mathcal{O} (\|\boldsymbol{\delta}\|^3) \quad (16)$$

and thus contains information about the geometry of the space distributions and the loss landscape. Additionally, when  $\boldsymbol{\theta}$  is a local minimum, the FIM is identical to the Hessian of the loss. The FIM is computed using gradients of the model on *a single datapoint* and specifically using only gradients of the output  $\nabla_{\boldsymbol{\theta}} \mathbf{f}_{\boldsymbol{\theta}}(\mathbf{x}_i)$ . For regression

$$\begin{aligned} \mathbf{F} &= \mathbb{E}_{\mathbf{x} \sim \mathcal{D}, \mathbf{y} \sim p_{\boldsymbol{\theta}}(\mathbf{y}|\mathbf{x})} (\nabla_{\boldsymbol{\theta}} \log(p_{\boldsymbol{\theta}}(\mathbf{y}|\mathbf{x})) \nabla_{\boldsymbol{\theta}} \log(p_{\boldsymbol{\theta}}(\mathbf{y}|\mathbf{x}))^\top) \\ &= \mathbb{E}_{\mathbf{x} \sim \mathcal{D}, \mathbf{y} \sim \mathcal{N}(\mathbf{y}; \mathbf{f}_{\boldsymbol{\theta}}(\mathbf{x}), \mathbf{I})} \left( \left( \nabla_{\boldsymbol{\theta}} \frac{1}{2} \|\mathbf{f}_{\boldsymbol{\theta}}(\mathbf{x}) - \mathbf{y}\|^2 \right) \left( \nabla_{\boldsymbol{\theta}} \frac{1}{2} \|\mathbf{f}_{\boldsymbol{\theta}}(\mathbf{x}) - \mathbf{y}\|^2 \right)^\top \right) \\ &= \mathbb{E}_{\mathbf{x} \sim \mathcal{D}} \left( \nabla_{\boldsymbol{\theta}} \mathbf{f}_{\boldsymbol{\theta}}(\mathbf{x}) \nabla_{\boldsymbol{\theta}} \mathbf{f}_{\boldsymbol{\theta}}(\mathbf{x})^\top \underbrace{\mathbb{E}_{\mathbf{y} \sim \mathcal{N}(\mathbf{y}; \mathbf{f}_{\boldsymbol{\theta}}(\mathbf{x}), \mathbf{I})} (\|\mathbf{f}_{\boldsymbol{\theta}}(\mathbf{x}) - \mathbf{y}\|^2)}_{\equiv \mathbf{I}} \right) \\ &= \mathbb{E}_{\mathbf{x} \sim \mathcal{D}} (\nabla_{\boldsymbol{\theta}} \mathbf{f}_{\boldsymbol{\theta}}(\mathbf{x}) \nabla_{\boldsymbol{\theta}} \mathbf{f}_{\boldsymbol{\theta}}(\mathbf{x})^\top), \end{aligned} \quad (17)$$

and for classification

$$\begin{aligned} \mathbf{F} &= \mathbb{E}_{\mathbf{x} \sim \mathcal{D}, \mathbf{y} \sim p_{\boldsymbol{\theta}}(\mathbf{y}|\mathbf{x})} (\nabla_{\boldsymbol{\theta}} \log(p_{\boldsymbol{\theta}}(\mathbf{y}|\mathbf{x})) \nabla_{\boldsymbol{\theta}} \log(p_{\boldsymbol{\theta}}(\mathbf{y}|\mathbf{x}))^\top) \\ &= \mathbb{E}_{\mathbf{x} \sim \mathcal{D}} \left( \sum_{k=1}^C p_{\boldsymbol{\theta}}(\mathbf{y} = k|\mathbf{x}) \nabla_{\boldsymbol{\theta}} \log(p_{\boldsymbol{\theta}}(\mathbf{y} = k|\mathbf{x})) \nabla_{\boldsymbol{\theta}} \log(p_{\boldsymbol{\theta}}(\mathbf{y} = k|\mathbf{x}))^\top \right) \\ &= \mathbb{E}_{\mathbf{x} \sim \mathcal{D}} \left( \sum_{k=1}^C \frac{1}{p_{\boldsymbol{\theta}}(\mathbf{y} = k|\mathbf{x})} \nabla_{\boldsymbol{\theta}} p_{\boldsymbol{\theta}}(\mathbf{y} = k|\mathbf{x}) \nabla_{\boldsymbol{\theta}} p_{\boldsymbol{\theta}}(\mathbf{y} = k|\mathbf{x})^\top \right) \end{aligned} \quad (18)$$

**The natural gradient.** The natural gradient is defined by preconditioning the gradient using the FIM

$$\nabla_{\text{nat}} := \mathbf{F}_{\boldsymbol{\theta}}^{-1} \nabla_{\boldsymbol{\theta}} \mathcal{L}(\boldsymbol{\theta}) \quad (19)$$

Motivated from the perspective of information geometry [4], the natural gradient defines the direction in parameter space that gives the largest change in the loss per unit of change in the *predictive distribution* of the model, measured by KL-divergence. This is to be contrasted with the standard gradient, which is the direction that gives the largest change in the loss per unit of change in *parameters*. Natural gradients are a fundamental tool in optimization and can be used to accelerate training [25, 27, 55].

Natural gradient optimization requires dynamic computation, storing and inversion the FIM whose size grows quadratically with the number of parameters, making it intractable at scale. This necessitates the use of approximations, such as K-FAC [26, 27, 55].

**FIM usage in pruning.** In pruning, we want to assign each weight of a trained model a saliency score that indicates its importance to the model's performance. The goal is to remove a certain percentage of weights with the lowest saliency, resulting in a compressed model with fewer parameters that still performs relatively well. The original OBD [45] and OBS [32] algorithms use the Hessian to compute saliency scores. However, since the model is trained, the parameters are likely close to a local minimum, and the the FIM is often used as an approximation of the Hessian.

Given parameters of a trained model  $\boldsymbol{\theta}$ , the OBD pruning saliency scores are given by

$$\boldsymbol{\theta}_{\text{OBD}} := \boldsymbol{\theta}^2 \odot \text{diag}(\mathbf{F}_{\boldsymbol{\theta}}), \quad (20)$$

where  $\boldsymbol{\theta}^2$  is a matrix of the square of each parameter, and  $\odot$  stands for point-wise product. The optimal brain surgeon (OBS) pruning saliency scores are given by

$$\boldsymbol{\theta}_{\text{OBS}} := \boldsymbol{\theta}^2 \oslash \text{diag}(\mathbf{F}_{\boldsymbol{\theta}}^{-1}), \quad (21)$$

where  $\oslash$  denotes point-wise division.

## B Extension to Transformers

In this section, we extend the results from the main text—originally detailed for MLPs—to transformer architectures. Similar extensions apply to a wide range of neural models, including CNNs, RNNs, and state-space models, as the key requirement is that the architecture consists of linear layers interleaved with nonlinearities. We begin by presenting the gradient decomposition for transformers, and then analyze its symmetry structure and the applicability of GradMetaNet.

### B.1 Gradient Decomposition for Transformers

As mentioned in Section 3, the gradient decomposition used in the paper generalizes to other types of neural architectures. For example, Grosse and Martens [27] discuss an extension to CNNs and Eschenhagen et al. [21] generalized this decomposition to other modern neural architectures, including transformers. Most transformer parameters are split between the fully-connected components (usually called FFNs or MLPs) and the attention layers. We have covered the MLP case in Section 3 and cover the rest in this section. Throughout this section use the following notation:

$$T = \text{sequence length}, d = d_{\text{model}}, h = \# \text{heads}, d_k = \frac{d}{h}, d_{\text{ff}} = \text{FFN expansion}, L = \# \text{blocks}.$$

For the reader’s convenience we use **brown** for transformer block indices, **blue** for attention head indices, and **green** for token indices. This notation and the notation for the rest of the section largely mirrors Vaswani et al. [83].

**Forward computation of transformer block  $l$ .** Table 3 details the forward pass of the  $l$ -th transformer block on an input sequence  $s = (x_1, \dots, x_T)$ .  $l$  is the index of the transformer block and  $j$  is the head index.

Table 3: Transformer forward-pass.

Object	Definition	Shape
Hidden input	$H^{(l-1)}$	$T \times d$
Queries	$Q^{(l,j)} = H^{(l-1)}W_Q^{(l,j)} + b_Q^{(l,j)}$	$T \times d_k$
Keys	$K^{(l,j)} = H^{(l-1)}W_K^{(l,j)} + b_K^{(l,j)}$	$T \times d_k$
Values	$V^{(l,j)} = H^{(l-1)}W_V^{(l,j)} + b_V^{(l,j)}$	$T \times d_k$
Attention weights	$A^{(l,j)} = \text{softmax}(Q^{(l,j)}K^{(l,j)\top} / \sqrt{d_k})$	$T \times T$
Head output	$O^{(l,j)} = A^{(l,j)}V^{(l,j)}$	$T \times d_k$
Merged heads	$O^{(l)} = [O^{(l,1)}, \dots, O^{(l,h)}]W_O^{(l)} + b_O^{(l)}$	$T \times d$
Post-MHA state	$\widehat{H}^{(l)} = \text{LayerNorm}(H^{(l-1)} + O^{(l)})$	$T \times d$
Feed-forward pre-act.	$P^{(l)} = \widehat{H}^{(l)}W_1^{(l)} + b_1^{(l)}$	$T \times d_{\text{ff}}$
Feed-forward out.	$U^{(l)} = \sigma(P^{(l)})W_2^{(l)} + b_2^{(l)}$	$T \times d$
Layer output	$H^{(l)} = \text{LayerNorm}(\widehat{H}^{(l)} + U^{(l)})$	$T \times d$

The transformer block parameters are presented in Table 4. Notes:

- In most implementations the key, query and value projection have no bias terms, i.e.

$$b_Q^{(l,j)} \equiv b_K^{(l,j)} \equiv b_V^{(l,j)} \equiv 0. \quad (22)$$

We include these bias terms for generality but they can be removed in most cases.

- Our derivation follows the *post-LayerNorm* (Post-LN) convention: residual add  $\rightarrow$  LayerNorm (as in the original transformers paper Vaswani et al. [83]). The analysis for Pre-LN transformers requires a slight adjustment to the derivation.
- Outside of the transformer block we would also typically have: the token embedding matrix  $E \in \mathbb{R}^{|\mathcal{V}| \times d}$ , positional embeddings  $\text{PE} \in \mathbb{R}^{T \times d}$  (or a sinusoidal schedule), and an unembedding matrix  $E^\top \in \mathbb{R}^{d \times |\mathcal{V}|}$ .

**Back-propagated (pre-activation) gradient signals.** Notice that all of the transformer parameters act as linear transformations (that are then sometimes passed Attention computations, LayerNorms, etc.). This means that we can use the observation from Appendix A.1 regarding gradient computation

Table 4: Transformer parameters.

Parameter	Description	Shape
$\mathbf{W}_Q^{(l,j)}$	query projection (head $j$ )	$d \times d_k$
$\mathbf{W}_K^{(l,j)}$	key projection (head $j$ )	$d \times d_k$
$\mathbf{W}_V^{(l,j)}$	value projection (head $j$ )	$d \times d_k$
$b_Q^{(l,j)}$	query bias	$d_k$
$b_K^{(l,j)}$	key bias	$d_k$
$b_V^{(l,j)}$	value bias	$d_k$
$\mathbf{W}_O^{(l)}$	output projection (concat. heads $\rightarrow d$ )	$(h d_k) \times d$
$b_O^{(l)}$	output bias	$d$
$\mathbf{W}_1^{(l)}$	FFN expansion ( $d \rightarrow d_{\text{ff}}$ )	$d \times d_{\text{ff}}$
$b_1^{(l)}$	FFN bias (layer 1)	$d_{\text{ff}}$
$\mathbf{W}_2^{(l)}$	FFN contraction ( $d_{\text{ff}} \rightarrow d$ )	$d_{\text{ff}} \times d$
$b_2^{(l)}$	FFN bias (layer 2)	$d$

for linear layers. Specifically, for every tensor computed in the transformer forward-pass (Table 3) that is the *output of a linear transformation*, we store the gradient w.r.t. that tensor:

$$\begin{aligned} \mathbf{g}_Q^{(l,j)} &= \frac{\partial \mathcal{L}_s}{\partial \mathbf{Q}^{(l,j)}}, & \mathbf{g}_K^{(l,j)} &= \frac{\partial \mathcal{L}_s}{\partial \mathbf{K}^{(l,j)}}, & \mathbf{g}_V^{(l,j)} &= \frac{\partial \mathcal{L}_s}{\partial \mathbf{V}^{(l,j)}}, \\ \mathbf{g}_O^{(l)} &= \frac{\partial \mathcal{L}_s}{\partial \mathbf{O}^{(l)}}, & \mathbf{g}_1^{(l)} &= \frac{\partial \mathcal{L}_s}{\partial \mathbf{P}^{(l)}}, & \mathbf{g}_2^{(l)} &= \frac{\partial \mathcal{L}_s}{\partial \mathbf{U}^{(l)}}. \end{aligned}$$

All of these tensors, referred to as *tangents*, share the same shapes as their forward counterparts.

**Outer-product parameter gradients.** Because every weight matrix appears in an affine map  $\mathbf{Y} = \mathbf{X}\mathbf{W} + \mathbf{b}$ , as analyzed in Appendix A.1, its gradient factorizes exactly into an *activation block*  $\mathbf{X}$  and a *tangent block*  $\mathbf{g}$ :

$$\nabla_{\mathbf{W}} \mathcal{L} = \mathbf{X}^\top \mathbf{g}, \quad \nabla_{\mathbf{b}} \mathcal{L} = \mathbf{g}^\top \mathbf{1}_{\textcolor{teal}{T}}. \quad (23)$$

Carrying this out for *all* parameters in the transformer block yields

$$\begin{aligned} \nabla_{\mathbf{W}_Q^{(l,j)}} \mathcal{L}_s &= (\mathbf{H}^{(l-1)})^\top \mathbf{g}_Q^{(l,j)}, & \nabla_{\mathbf{b}_Q^{(l,j)}} \mathcal{L}_s &= (\mathbf{g}_Q^{(l,j)})^\top \mathbf{1}_{\textcolor{teal}{T}}, \\ \nabla_{\mathbf{W}_K^{(l,j)}} \mathcal{L}_s &= (\mathbf{H}^{(l-1)})^\top \mathbf{g}_K^{(l,j)}, & \nabla_{\mathbf{b}_K^{(l,j)}} \mathcal{L}_s &= (\mathbf{g}_K^{(l,j)})^\top \mathbf{1}_{\textcolor{teal}{T}}, \\ \nabla_{\mathbf{W}_V^{(l,j)}} \mathcal{L}_s &= (\mathbf{H}^{(l-1)})^\top \mathbf{g}_V^{(l,j)}, & \nabla_{\mathbf{b}_V^{(l,j)}} \mathcal{L}_s &= (\mathbf{g}_V^{(l,j)})^\top \mathbf{1}_{\textcolor{teal}{T}}, \\ \nabla_{\mathbf{W}_O^{(l)}} \mathcal{L}_s &= [\mathbf{O}^{(l,1)}, \dots, \mathbf{O}^{(l,h)}]^\top \mathbf{g}_O^{(l)}, & \nabla_{\mathbf{b}_O^{(l)}} \mathcal{L}_s &= (\mathbf{g}_O^{(l)})^\top \mathbf{1}_{\textcolor{teal}{T}}, \\ \nabla_{\mathbf{W}_1^{(l)}} \mathcal{L}_s &= (\widehat{\mathbf{H}}^{(l)})^\top \mathbf{g}_1^{(l)}, & \nabla_{\mathbf{b}_1^{(l)}} \mathcal{L}_s &= (\mathbf{g}_1^{(l)})^\top \mathbf{1}_{\textcolor{teal}{T}}, \\ \nabla_{\mathbf{W}_2^{(l)}} \mathcal{L}_s &= \sigma(\mathbf{P}^{(l)})^\top \mathbf{g}_2^{(l)}, & \nabla_{\mathbf{b}_2^{(l)}} \mathcal{L}_s &= (\mathbf{g}_2^{(l)})^\top \mathbf{1}_{\textcolor{teal}{T}}. \end{aligned}$$

**Token-wise view (“sum of rank-1” form).** Unfolding, for example,

$$\nabla_{\mathbf{W}_Q^{(l,j)}} = (\mathbf{H}^{(l-1)})^\top \mathbf{g}_Q^{(l,j)} = \sum_{t=1}^{\textcolor{teal}{T}} (\mathbf{g}_Q^{(l,j)})_t (\mathbf{H}_t^{(l-1)})^\top, \quad (24)$$

reveals that *each weight gradient is a sum of  $\textcolor{teal}{T}$  rank-1 outer products*. Storing the pair  $(\mathbf{H}_t^{(l-1)}, \mathbf{g}_{Q,t}^{(l,j)})$  for every token  $t$  is therefore sufficient to reconstruct  $\nabla_{\mathbf{W}_Q^{(l,j)}} \mathcal{L}_s$  exactly, and identical statements hold for  $\mathbf{W}_K^{(l,j)}, \mathbf{W}_V^{(l,j)}, \mathbf{W}_O^{(l)}, \mathbf{W}_1^{(l)}$ , and  $\mathbf{W}_2^{(l)}$ .

**Compact gradient representation.** For transformer block  $l = 1, \dots, L$ , and head  $j = 1, \dots, h$ , define:

$$\begin{aligned}\mathbf{g}_{\text{res}}^{(l)} &:= (\underbrace{\mathbf{H}^{(l-1)}}_{\text{activation}}, \underbrace{\mathbf{g}_O^{(l)}}_{\substack{\text{attn. out.} \\ \text{tangents}}}, \underbrace{\widehat{\mathbf{H}}^{(l)}}, \underbrace{\mathbf{g}_2^{(l)}}_{\substack{\text{post-LN} \\ \text{FFN}_2 \\ \text{tangents}}}) \in \Gamma_{\text{T}}^{\text{res}} := \mathbb{R}^{T \times d \times 4}, \\ \mathbf{g}_{\text{attn}}^{(l)} &:= (\underbrace{\mathbf{g}_Q^{(l,1:h)}}_{\text{query tangents}}, \underbrace{\mathbf{g}_K^{(l,1:h)}}_{\text{key tangents}}, \underbrace{\mathbf{g}_V^{(l,1:h)}}_{\text{value tangents}}, \underbrace{\mathbf{O}^{(l,1:h)}}_{\text{MHA outputs}}) \in \Gamma_{\text{T}}^{\text{attn}} := \mathbb{R}^{T \times (hd_k) \times 4}, \\ \mathbf{g}_{\text{hidden}}^{(l)} &:= (\underbrace{\sigma(\mathbf{P}^{(l)})}_{\text{hidden rep.}}, \underbrace{\mathbf{g}_1^{(l)}}_{\substack{\text{FFN}_1 \\ \text{tangents}}}) \in \Gamma_{\text{T}}^{\text{hidden}} := \mathbb{R}^{T \times d_{\text{ff}} \times 2},\end{aligned}\quad (25)$$

Collecting the whole set, we get the tensors

$$\mathbf{g}^{(l)} = (\mathbf{g}_{\text{res}}^{(l)}, \mathbf{g}_{\text{attn}}^{(l)}, \mathbf{g}_{\text{hidden}}^{(l)}) \in \Gamma_{\text{T}}^{(l)} := \Gamma_{\text{T}}^{\text{res}} \oplus \Gamma_{\text{T}}^{\text{attn}} \oplus \Gamma_{\text{T}}^{\text{hidden}}, \quad (26)$$

and

$$\mathbf{g} := (\mathbf{g}^{(1)}, \dots, \mathbf{g}^{(L)}) \in \Gamma_{\text{T}} := \Gamma_{\text{T}}^{(1)} \oplus \dots \oplus \Gamma_{\text{T}}^{(L)}. \quad (27)$$

## B.2 Transformer (Decomposed) Gradient Symmetries

The permutation symmetry groups of the parameter spaces of general architectures, and transformers in particular, were analyzed in Kofinas et al. [41], Lim et al. [48], Zhou et al. [91]. Kofinas et al. [41], Lim et al. [48] identify permutation symmetries with automorphisms of the computation graph of  $\mathbf{f}_{\theta}$ , and Zhou et al. [91] analyzes the permutation symmetries of multi-dimensional tensors. To give a flavor of the adaptations needed in the transformer case, we first look at the effects of the residual connections. Intuitively, we need to tie together the neuron spaces of dimension  $d$  (i.e.  $\mathbf{H}^{(l-1)}$ ,  $\mathbf{O}^{(l)}$ ,  $\widehat{\mathbf{H}}^{(l)}$ , and  $\mathbf{U}^{(l)}$ ) under the same symmetry group ( $S_d$ ) because of the residual connections. With this “symmetry tying” the residual connections and LayerNorms preserve permutation symmetries, since if  $\Phi, \Psi : \mathbb{R}^d \rightarrow \mathbb{R}^d$  are  $S_d$ -equivariant functions, we have

$$(\Phi + \Psi)(\sigma \cdot \mathbf{x}) = \Phi(\sigma \cdot \mathbf{x}) + \Psi(\sigma \cdot \mathbf{x}) = \sigma \cdot \Phi(\mathbf{x}) + \sigma \cdot \Psi(\mathbf{x}) = \sigma \cdot (\Phi(\mathbf{x}) + \Psi(\mathbf{x})) = \sigma \cdot (\Phi + \Psi)(\mathbf{x}),$$

and

$$\text{LayerNorm}(\sigma \cdot \mathbf{x}) = \sigma \cdot \text{LayerNorm}(\mathbf{x}).$$

The analysis of the permutation symmetry group of transformer weight spaces provided in Kofinas et al. [41], Lim et al. [48], Zhou et al. [91] follows similar observations. The resulting symmetry group is

$$G = \underbrace{S_{\text{T}}}_{\text{tokens}} \times \underbrace{S_d}_{\text{residual stream}} \times \underbrace{\overbrace{(S_{d_k})^h}^{\times L \text{ transformer blocks}}}_{\text{MHA output}} \times \underbrace{S_{d_{\text{ff}}}}_{\text{FFN hidden dim}}. \quad (28)$$

Where, in our decomposed gradients case,  $S_{\text{T}}$  acts on the sequence dimension of all spaces,  $S_d$  acts on the second axis (the  $d$ -dimension) of all  $\Gamma_{\text{T}}^{\text{res}}$ s, each  $(S_{d_k})^h$  acts independently on the  $V^{(l,j)}$  and  $O^{(l,j)}$  components of each head in  $\Gamma_{\text{T}}^{\text{attn}}$ , and each  $S_{d_{\text{ff}}}$  acts on the hidden dimension of the FFN represented in  $\Gamma_{\text{T}}^{\text{hidden}}$ .

We note that transformer parameter spaces exhibit other neural symmetries that are not modeled by the *permutation* symmetry group  $G$ . These symmetries include ReLU scaling symmetries [38] and general attention symmetries (the transformation  $(\mathbf{Q}^{(l,j)}, \mathbf{K}^{(l,j)}) \mapsto (\mathbf{Q}^{(l,j)} \mathbf{R}, \mathbf{K}^{(l,j)} \mathbf{R}^{-\top})$  for  $\mathbf{R} \in \text{GL}_{d_k}(\mathbb{R})$  results in the same attention matrix). Accounting for these symmetries is left for future work.

## B.3 Adapting GradMetaNet to Transformers

To implement a GradMetaNet version that can process transformer gradients we need to make the following adaptions. First, we treat the sequence dimension as a batch dimension, optionally with additional positional encoding for the token index. Note that this positional encoding is not strictly required since, as can be seen in Equation 24, the full gradient is a sum over the rank-1 components and is therefore an  $S_{\text{T}}$ -invariant function of them. We then treat  $\Gamma_{\text{T}}^{\text{res}}$ ,  $\Gamma_{\text{T}}^{\text{attn}}$ , and  $\Gamma_{\text{T}}^{\text{hidden}}$  as we treat neuron spaces with an additional positional encoding for each attention head to convert the  $S_{(h d_k)}$ -

equivariance of  $L_\Gamma$  to  $(S_{d_k})^{\textcolor{blue}{b}}$ -equivariance. As mentioned in Appendix B.2 we treat the  $\textcolor{red}{L}$  copies of  $\Gamma_{\textcolor{teal}{T}}^{\text{res}}$  as a single neuron space, since the symmetry structure of the residual stream is tied together.

## C Gradient and Weight Spaces

This section formally defines the vector spaces used to represent (sets of) gradients and weights. For batch size  $\textcolor{brown}{b}$  and feature dimension  $\textcolor{violet}{f}$ , the feature vector spaces  $\Gamma[\textcolor{violet}{f}]$  and  $\Gamma_{\textcolor{brown}{b}}[\textcolor{violet}{f}]$ ,  $\Theta[\textcolor{violet}{f}]$ , and  $\Theta_{\textcolor{brown}{b}}[\textcolor{violet}{f}]$  are defined by

$$\begin{aligned}\Gamma[\textcolor{violet}{f}] &:= \Gamma^{(0)}[\textcolor{violet}{f}] \oplus \cdots \oplus \Gamma^{(\textcolor{red}{L})}[\textcolor{violet}{f}] \\ \Gamma_{\textcolor{brown}{b}}[\textcolor{violet}{f}] &:= \Gamma_{\textcolor{brown}{b}}^{(0)}[\textcolor{violet}{f}] \oplus \cdots \oplus \Gamma_{\textcolor{brown}{b}}^{(\textcolor{red}{L})}[\textcolor{violet}{f}] \\ \Theta[\textcolor{violet}{f}] &:= \mathcal{W}^{(1)}[\textcolor{violet}{f}] \oplus \mathcal{U}^{(1)}[\textcolor{violet}{f}] \oplus \cdots \oplus \mathcal{W}^{(\textcolor{red}{L})}[\textcolor{violet}{f}] \oplus \mathcal{U}^{(\textcolor{red}{L})}[\textcolor{violet}{f}] \\ \Theta_{\textcolor{brown}{b}}[\textcolor{violet}{f}] &:= \mathcal{W}_{\textcolor{brown}{b}}^{(1)}[\textcolor{violet}{f}] \oplus \mathcal{U}_{\textcolor{brown}{b}}^{(1)}[\textcolor{violet}{f}] \oplus \cdots \oplus \mathcal{W}_{\textcolor{brown}{b}}^{(\textcolor{red}{L})}[\textcolor{violet}{f}] \oplus \mathcal{U}_{\textcolor{brown}{b}}^{(\textcolor{red}{L})}[\textcolor{violet}{f}]\end{aligned}\tag{29}$$

where,

$$\begin{aligned}\Gamma^{(\textcolor{red}{l})}[\textcolor{violet}{f}] &:= \mathbb{R}^{d_l \times \textcolor{violet}{f}}, \Gamma_{\textcolor{brown}{b}}^{(\textcolor{red}{l})}[\textcolor{violet}{f}] := \mathbb{R}^{\textcolor{brown}{b} \times d_l \times \textcolor{violet}{f}} \\ \mathcal{W}^{(\textcolor{red}{l})}[\textcolor{violet}{f}] &:= \mathbb{R}^{d_l \times d_{l-1} \times \textcolor{violet}{f}}, \mathcal{W}_{\textcolor{brown}{b}}^{(\textcolor{red}{l})}[\textcolor{violet}{f}] := \mathbb{R}^{\textcolor{brown}{b} \times d_l \times d_{l-1} \times \textcolor{violet}{f}} \\ \mathcal{U}^{(\textcolor{red}{l})}[\textcolor{violet}{f}] &:= \mathbb{R}^{d_l \times \textcolor{violet}{f}}, \mathcal{U}_{\textcolor{brown}{b}}^{(\textcolor{red}{l})}[\textcolor{violet}{f}] := \mathbb{R}^{\textcolor{brown}{b} \times d_l \times \textcolor{violet}{f}}\end{aligned}\tag{30}$$

Note that  $\Gamma[2] = \Gamma$ ,  $\Gamma_{\textcolor{brown}{b}}[2] = \Gamma_{\textcolor{brown}{b}}$ ,  $\Theta[1] = \Theta$  and  $\Theta_{\textcolor{brown}{b}}[1] = \Theta_{\textcolor{brown}{b}}$ .

## D Architecture Details

The following is a detailed description of each of the layers used in GradMetaNet.

### D.1 GradMetaNet

**The positional encoding map.** Similarly to Lim et al. [48], Zhou et al. [92], we use a positional encoding map  $\text{PE} : \Gamma_b \rightarrow \Gamma_b[\textcolor{violet}{f}]$  that concatenates a layer identifier to neurons in intermediate layers and a neuron identifier to each neuron in the first and last layers, i.e.

$$\begin{aligned}\text{PE}(\mathbf{g}^{(0)})_{i,j,:} &= \left[ \mathbf{g}_{i,j,:}^{(0)}, \mathbf{e}_{\text{in}}(j) \right], \\ \text{PE}(\mathbf{g}^{(l)})_{i,j,:} &= \left[ \mathbf{g}_{i,j,:}^{(l)}, \mathbf{e}_{\text{layer}}(l) \right], \quad \text{for } l = 1, \dots, L-1, \\ \text{PE}(\mathbf{g}^{(L)})_{i,j,:} &= \left[ \mathbf{g}_{i,j,:}^{(L)}, \mathbf{e}_{\text{out}}(j) \right],\end{aligned}$$

where  $[\cdot, \cdot]$  denotes concatenation along the feature axis.  $\mathbf{e}_{\text{in}}$  and  $\mathbf{e}_{\text{out}}$  assign unique identifiers to each neuron in the input and output layers respectively, and  $\mathbf{e}_{\text{layer}}$  assigns unique identifiers to each hidden layer. We implement all encoding maps using sinusoidal positional encoding [79].

**Gradient-set-to-gradient-set layers.**  $L_{\Gamma_b} : \Gamma_b[f_{\text{in}}] \rightarrow \Gamma_b[f_{\text{out}}]$  are parametrized similarly to the interactions-across-sets layers introduced in Hartford et al. [31], and are implemented as

$$L_{\Gamma_b} \left( \mathbf{g}^{(l)} \right)_{i,j,:} = M_1 \mathbf{g}_{i,j,:}^{(l)} + M_2 \sum_{i'=1}^b \mathbf{g}_{i',j,:}^{(l)} + M_3 \sum_{l'=0}^L \sum_{j'=1}^{d_l} \mathbf{g}_{i,j',:}^{(l')} + M_4 \sum_{l'=0}^L \sum_{i'=1}^b \sum_{j'=1}^{d_{l'}} \mathbf{g}_{i',j',:}^{(l')}, \tag{31}$$

for learnable  $M_1, M_2, M_3, M_4 \in \mathbb{R}^{f_{\text{out}} \times f_{\text{in}}}$ .

**Gradient-set-to-gradient pooling layer.**  $L_{\text{Pool}} : \Gamma_b[f_{\text{in}}] \rightarrow \Gamma[f_{\text{out}}]$  is implemented as

$$L_{\text{Pool}} \left( \mathbf{g}^{(l)} \right)_{j,:} = M_1 \sum_{i'=1}^b \mathbf{g}_{i',j,:}^{(l)} + M_2 \sum_{l'=0}^L \sum_{i'=1}^b \sum_{j'=1}^{d_{l'}} \mathbf{g}_{i',j',:}^{(l')}, \tag{32}$$

for learnable  $M_1, M_2 \in \mathbb{R}^{f_{\text{out}} \times f_{\text{in}}}$ .

**Gradient-to-gradient layers.**  $L_\Gamma : \Gamma[f_{\text{in}}] \rightarrow \Gamma[f_{\text{out}}]$  are parameterized as equivariant DeepSets networks [90], and take the form

$$L_\Gamma(\mathbf{g}^{(l)})_{i,:} = M_1 \mathbf{g}_{i,:}^{(l)} + M_2 \sum_{l'=1}^L \sum_{i'=1}^{d_l} \mathbf{g}_{i',:}^{(l')}, \quad (33)$$

for learnable  $M_1, M_2 \in \mathbb{R}^{f_{\text{out}} \times f_{\text{in}}}$ .

**Gradient-to-weight component.** Similarly to the generalized product layer in Navon et al. [61],  $L_{\text{Prod}} : \Gamma[f_{\text{in}}] \rightarrow \Theta$  applies a pointwise MLP to the features associated with the neurons connected to each weight, or in the case of biases, to the feature vectors corresponding to the respective neuron.

$$\mathbf{W}_{i,j}^{(l)} = \text{MLP}_1([\mathbf{g}_{i,:}^{(l)}, \mathbf{g}_{j,:}^{(l+1)}]), \mathbf{b}_i^{(l)} = \text{MLP}_2(\mathbf{g}_{i,:}^{(l)}). \quad (34)$$

## D.2 GradMetaNet++

Similarly to GradMetaNet, A GradMetaNet++ model  $\Phi$  comprises of updates of different types: a positional encoding layer PE, gradient-set-to-gradient-set updates  $U_{\Gamma_b}$ , and a gradient-set-to-weight component  $U_{\text{Prod}}$ . A GradMetaNet++ model is parameterized as

$$\Phi = U_{\text{Prod}} \circ U_{\Gamma_b}^{(k)} \circ \dots \circ U_{\Gamma_b}^{(1)} \circ \text{PE}. \quad (35)$$

We now describe each of these layers.

**The positional encoding map.** The positional encoding map used for GradMetaNet++ is identical to the one used in GradMetaNet and described in Section 5.

**Gradient-sets-to-gradient-set updates.**  $U_{\Gamma_b} : \Gamma_b[f_{\text{in}}] \rightarrow \Gamma_b[f_{\text{out}}]$  Are attention variants of the  $L_{\Gamma_b}$  layers decribed in Section 5. For a given  $\mathbf{g} \in \Gamma_b[f_{\text{in}}]$  in order to compute  $U_{\Gamma_b}(\mathbf{g})$  we first compute set-wise attention, given by:

$$\text{Attention}_b^h(\mathbf{g})_{i,j,:}^{(l)} = \sum_{j=1}^b \text{softmax} \left( \frac{\langle M_Q^h \mathbf{g}_{k,j,:}^{(l)}, M_K^h \mathbf{g}_{i,j,:}^{(l)} \rangle}{\sqrt{f_{\text{in}}}} \right) M_V^h \mathbf{g}_{k,j,:}^{(l)}. \quad (36)$$

$$\text{Attention}_b(\mathbf{g})_{i,j,:}^{(l)} = M_O[\text{Attention}_b^1(\mathbf{g})_{i,j,:}^{(l)}, \dots, \text{Attention}_b^H(\mathbf{g})_{i,j,:}^{(l)}] \quad (37)$$

Here  $\langle \cdot, \cdot \rangle$  denotes inner product and  $M_K^h, M_Q^h, M_V^h \in \mathbb{R}^{f_{\text{in}} \times f_{\text{in}}}$  are learnable matrices used in each attention head and  $M_O \in \mathbb{R}^{f_{\text{in}}^H \times f_{\text{out}}}$  is a final aggregation linear layer. We then compute gradient-wise attention, given by:

$$\text{Attention}_g^h(\mathbf{g})_{i,j,:}^{(l)} = \sum_{l'=0}^L \sum_{k=1}^{d_{l'}} \text{softmax} \left( \frac{\langle M_Q^h \mathbf{g}_{i,k,:}^{(l')}, M_K^h \mathbf{g}_{i,j,:}^{(l)} \rangle}{\sqrt{f_{\text{in}}}} \right) M_V^h \mathbf{g}_{i,k,:}^{(l')}. \quad (38)$$

$$\text{Attention}_g(\mathbf{g})_{i,j,:}^{(l)} = M_O[\text{Attention}_g^1(\mathbf{g})_{i,j,:}^{(l)}, \dots, \text{Attention}_g^H(\mathbf{g})_{i,j,:}^{(l)}] \quad (39)$$

Here we slightly abuse notation and denote by  $M_K^h, M_Q^h, M_V^h \in \mathbb{R}^{f_{\text{in}} \times f_{\text{in}}}$ ,  $M_O \in \mathbb{R}^{f_{\text{in}}^H \times f_{\text{out}}}$  learnable matrices different from those in equations 36 and 37. finally, the value of  $U_{\Gamma_b}(\mathbf{g})$  is given by

$$U_{\Gamma_b}(\mathbf{g})_{i,j,:}^{(l)} = \text{MLP}(\mathbf{g}_{i,j,:}^{(l)} + \text{Attention}_b(\mathbf{g})_{i,j,:}^{(l)} + \text{Attention}_g(\mathbf{g})_{i,j,:}^{(l)}). \quad (40)$$

**Gradient-batch-to-weight update.** As GradMetaNet++ prioritizes empirical improvements over computational efficiency, we directly use a gradient-batch-to-weight update, which we found to yield better performance.

The gradient-to-weight mapping,  $U_{\text{Prod}} : \Gamma_b[f_{\text{in}}] \rightarrow \Theta$ , applies a pointwise MLP to the feature vectors associated with the neurons connected to each weight in every element of the batch. In the case of biases, the MLP is applied to the feature vectors corresponding to the respective neuron.

Finally, the results are summed across the batch. Formally, this can be expressed by  $U_{\text{Prod}}(\mathbf{g}) = (\mathbf{W}_1, \mathbf{b}_1 \dots, \mathbf{W}_L, \mathbf{b}_L)$  where:

$$(\mathbf{W}_l)_{i,j} = \sum_{k=1}^b \text{MLP}_1([\mathbf{g}_{k,i,:}^{(l)}, \mathbf{g}_{k,j,:}^{(l+1)}]), (\mathbf{b}_l)_i = \sum_{k=1}^b \text{MLP}_2(\mathbf{g}_{k,i,:}^{(l)}). \quad (41)$$

### D.3 Invariant GradMetaNet.

In some cases (e.g. evaluating influence functions) we want GradMetaNet to output a single invariant vector  $\in \mathbb{R}^{f_{\text{out}}}$  rather than a parameter vector  $\in \Theta$ . In this case we replace the  $L_{\text{Prod}}$  component described in Section 5 with a  $L_{\text{Vec}}$  layer described below. For an element  $\mathbf{g} \in \Gamma[f_{\text{in}}]$ ,

$$L_{\text{Vec}}(\mathbf{g}) = M \sum_{l'=1}^L \sum_{i'=1}^{d_l} \mathbf{g}_{i',:}^{(l')}. \quad (42)$$

Where  $M \in \mathbb{R}^{f_{\text{out}} \times f_{\text{in}}}$  is a learnable matrix. This results in invariant vector outputs.

### D.4 Computational Complexity.

We analyze the space and runtime complexity of GradMetaNet and GradMetaNet++, comparing them to alternative approaches. Throughout this discussion we denote by  $P$  the number of parameters in the underlying MLP  $f_{\theta}$ , whose gradients are being processed, and denote the number of neurons by  $N$ . Since the gradient-batch-to-gradient-batch update is the most computationally intensive component in both architectures, we focus our analysis on this operation.

**GradMetaNet.** The gradient-batch-to-gradient-batch update in GradMetaNet consists of a stack of layers  $L_{\Gamma_b} : \Gamma_b[f_{\text{in}}] \rightarrow \Gamma_b[f_{\text{out}}]$ , as defined in Section 5. Each of these layers has both space and runtime complexity of  $O(N \cdot b \cdot f_{\text{in}} \cdot f_{\text{out}})$ . Thus, assuming a fixed hidden dimension and number of layers, GradMetaNet has a complexity of  $O(N \cdot b)$ .

**Gradient concatenation and averaging in weight space.** Both gradient concatenation and averaging methods process sets of gradients by utilizing weight-space architectures, such as those introduced by Lim et al. [48], Navon et al. [60]. These architectures employ layers  $L_w : \Theta[f_{\text{in}}] \rightarrow \Theta[f_{\text{out}}]$  with time and space complexity  $O(P \cdot f_{\text{in}} \cdot f_{\text{out}})$ .

In the *concatenation* approach, gradients are concatenated, producing an input element in  $\Theta[b]$ , resulting in an overall complexity of  $O(P \cdot b)$  for a fixed hidden dimension and number of layers. This approach scales poorly compared to GradMetaNet when  $b \cdot P > b \cdot N$ . In contrast, the *averaging* approach reduces gradients to a single representation in  $\Theta[1]$ , yielding a complexity of  $O(P)$ . However, this method is also suboptimal in the overparameterized regime ( $P > b \cdot N$ ). In addition, even in cases where the batch size is sufficiently large such that  $P < b \cdot N$ , gradient-averaging methods may still be suboptimal due to their expressivity limitations (see Section 6).

**GradMetaNet++.** The gradient-batch-to-gradient-batch update in GradMetaNet++ is implemented using a stack of layers  $U_{\Gamma_b} : \Gamma_b[f_{\text{in}}] \rightarrow \Gamma_b[f_{\text{out}}]$ , as detailed in Appendix D.2. Each layer has a time complexity of  $O((N^2 \cdot b + b^2 \cdot N) \cdot f_{\text{in}} \cdot f_{\text{out}})$  and can be designed to achieve a space complexity of  $O(N \cdot b \cdot f_{\text{in}} \cdot f_{\text{out}})$ . While these layers have the highest time complexity among the approaches considered so far, their space complexity remains efficient. Moreover, constructing an attention-based variant for weight-space architectures would scale quadratically with  $P$ , making it far less practical in terms of scalability.

## E Theory

In this section we provide proofs and further discussion for the results presented in Section 6. Throughout this section we use  $\nabla_i$  to denote gradients of the networks computed on a single datapoint.

## E.1 Importance of Processing Collections of Gradients

In Section 6, we discuss the expressivity limitations of processing the gradient of the average loss on the batch compared to the collection of gradient at each of the datapoints. In this section we formalize these limitations. We start with some notation and definitions. As we saw in Appendix A.3, the FIM can be computed using gradients on individual datapoints. Given a set of such gradients  $\mathcal{G} = \{\nabla_1, \dots, \nabla_b\}$ , the FIM computed using the gradients in  $\mathcal{G}$  is denoted by  $\mathbf{F}_{\mathcal{G}}$ . As we saw in the main text  $\mathcal{G}$  can be thought of as an element of  $\Theta_b$ .

**Definition 4.** Let  $\Phi : \Theta \times \Theta_b \rightarrow \Theta$  be a function whose inputs are parameters  $\theta$  and a set of gradients  $\mathcal{G} = \{\nabla_1, \dots, \nabla_b\}$ . We say that  $\Phi$  non-trivially depends on the FIM if for some function  $\Psi : (\Theta \otimes \Theta) \times \Theta \times \Theta \rightarrow \Theta$ ,

$$\Phi(\theta, \mathcal{G}) = \Psi\left(\mathbf{F}_{\mathcal{G}}, \theta, \frac{1}{b} \sum_{i=1}^b \nabla_i\right) \quad (43)$$

and there exists a pair of inputs  $\theta, \mathcal{G} = \{\nabla_1, \dots, \nabla_b\}$  and  $\theta', \mathcal{G}' = \{\nabla'_1, \dots, \nabla'_b\}$  where  $\mathcal{G}$  and  $\mathcal{G}'$  are admissible gradient sets<sup>3</sup> and such that  $\theta = \theta', \frac{1}{b} \sum_{i=1}^b \nabla_i = \frac{1}{b} \sum_{i=1}^b \nabla'_i$  but

$$\Phi(\theta, \mathcal{G}) = \Psi\left(\mathbf{F}_{\mathcal{G}}, \theta, \frac{1}{b} \sum_{i=1}^b \nabla_i\right) \neq \Psi\left(\mathbf{F}_{\mathcal{G}'}, \theta', \frac{1}{b} \sum_{i=1}^b \nabla'_i\right) = \Phi(\theta', \mathcal{G}'). \quad (44)$$

Many commonly used functions over sets of gradients non-trivially depend on the FIM. before providing such examples, we first state the following trivial proposition.

**Proposition 5.** Let  $\Phi : \Theta \times \Theta_b \rightarrow \Theta$  be a function that non-trivially depends on the FIM. There exist an  $\epsilon > 0$  such that for any continuous function  $\Lambda : \Theta \times \Theta \rightarrow \Theta$  it holds that:

$$\max_{\theta, \mathcal{G}} \left\| \Phi(\theta, \mathcal{G}) - \Lambda\left(\theta, \frac{1}{b} \sum \nabla_i\right) \right\| > \epsilon. \quad (45)$$

In other words, functions which non-trivially depend on the FIM cannot be approximated (in the  $\ell_\infty$ -sense) by continuous functions that rely only on the average gradient.

*Proof.* The proof follows trivially from Definition 4. Let  $\theta, \mathcal{G} = \{\nabla_1, \dots, \nabla_b\}$  and  $\theta', \mathcal{G}' = \{\nabla'_1, \dots, \nabla'_b\}$  be a pair of inputs such that  $\theta = \theta'$  and  $\frac{1}{b} \sum_{i=1}^b \nabla_i = \frac{1}{b} \sum_{i=1}^b \nabla'_i$ , but

$$\Phi(\theta, \mathcal{G}) \neq \Phi(\theta', \mathcal{G}') \quad (46)$$

For any  $\Lambda : \Theta \times \Theta \rightarrow \Theta$  we have

$$\Lambda\left(\theta, \frac{1}{b} \sum \nabla_i\right) = \Lambda\left(\theta', \frac{1}{b} \sum \nabla'_i\right). \quad (47)$$

Therefore, if we choose  $0 < \epsilon < 2\|\Phi(\theta, \mathcal{G}) - \Phi(\theta', \mathcal{G}')\|$  we have

$$\|\Phi(\theta, \mathcal{G}) - \Lambda\left(\theta, \frac{1}{b} \sum \nabla_i\right)\| + \|\Phi(\theta', \mathcal{G}') - \Lambda\left(\theta', \frac{1}{b} \sum \nabla'_i\right)\| \geq \|\Phi(\theta, \mathcal{G}) - \Phi(\theta', \mathcal{G}')\| > 2\epsilon. \quad (48)$$

This implies that either  $\|\Phi(\theta, \mathcal{G}) - \Lambda\left(\theta, \frac{1}{b} \sum \nabla_i\right)\| > \epsilon$  or  $\|\Phi(\theta', \mathcal{G}') - \Lambda\left(\theta', \frac{1}{b} \sum \nabla'_i\right)\| > \epsilon$  and so

$$\max_{\theta, \mathcal{G}} \|\Phi(\theta, \mathcal{G}) - \Lambda\left(\theta, \frac{1}{b} \sum \nabla_i\right)\| > \epsilon \quad (49)$$

completing the proof.  $\square$

We want to show that the computation of the natural gradient and the OBD/OBS pruning saliency scores non-trivially depends of the FIM. To do so we first formally define these computations as functions over  $\Theta_b$ .

**Definition 6** (Natural gradient map). The natural gradient map  $\Phi_{\text{nat}} : \Theta \times \Theta_b \rightarrow \Theta$  is defined by

$$\Phi_{\text{nat}}(\nabla, \mathcal{G}) = (\mathbf{F}_{\mathcal{G}} + \epsilon \mathbf{I})^{-1} \nabla, \quad (50)$$

<sup>3</sup>Here, by ‘‘admissible’’, we mean that the elements of  $\mathcal{G}$  and  $\mathcal{G}'$  are actual MLP gradients, rather than arbitrary elements of  $\Theta$ .

where  $\mathbf{I}$  is the identity matrix and  $\epsilon > 0$  is a damping factor. These are added since while positive-definite, the FIM is not guaranteed to be invertible.

**Definition 7** (OBD/OBS pruning saliency maps). The OBD saliency map  $\Phi_{\text{OBD}} : \Theta \times \Theta_b \rightarrow \Theta$  is defined by

$$\Phi_{\text{OBD}}(\theta, \mathcal{G}) := \theta^2 \odot \text{diag}(\mathbf{F}_{\mathcal{G}}). \quad (51)$$

The OBS saliency map  $\Phi_{\text{OBS}} : \Theta \times \Theta_b \rightarrow \Theta$  is defined by

$$\Phi_{\text{OBS}}(\theta, \mathcal{G}) := \theta^2 \oslash \text{diag}((\mathbf{F}_{\mathcal{G}} + \epsilon \mathbf{I})^{-1}). \quad (52)$$

We now show that both the natural gradient map and the OBD/OBS pruning saliency maps non-trivially depend on the FIM.

**Proposition 8.** *The maps  $\Phi_{\text{nat}}$ ,  $\Phi_{\text{OBD}}$ , and  $\Phi_{\text{OBS}}$  non-trivially depend on the FIM.*

*Proof.* To start, we assume that  $f_{\theta}$  is a single-layer MLP, i.e. a linear map from the input space  $\mathbb{R}^n$  to the output space  $\mathbb{R}$ . The proof can be extended to deeper MLPs by composing the linear map with an MLP implements the identity function. Given a batch of datapoints  $\mathcal{D} = \{(\mathbf{x}_1, \mathbf{y}_1), \dots, (\mathbf{x}_N, \mathbf{y}_N)\} \subset \mathbb{R}^n \times \mathbb{R}$ , the gradients of the output are

$$\nabla_i = \nabla_{\theta} f_{\theta}(\mathbf{x}_i) = \mathbf{x}_i. \quad (53)$$

Thus, as discussed in Appendix A.3, the FIM on  $\mathcal{G} = \{\nabla_1, \dots, \nabla_n\}$  can be computed as

$$\mathbf{F}_{\mathcal{G}} = \frac{1}{b} \sum_{i=1}^b \mathbf{x}_i \mathbf{x}_i^{\top}. \quad (54)$$

We begin by showing that  $\Phi_{\text{nat}}$  non-trivially depends on the FIM. This is equivalent to showing that there exist two choices  $\mathcal{B} = \{(\mathbf{x}_1, \mathbf{y}_1), \dots, (\mathbf{x}_b, \mathbf{y}_b)\}$ ,  $\mathcal{B}' = \{(\mathbf{x}'_1, \mathbf{y}'_1), \dots, (\mathbf{x}'_b, \mathbf{y}'_b)\}$  with corresponding gradients  $\mathcal{G} = \{\nabla_1, \dots, \nabla_b\}$ ,  $\mathcal{G}' = \{\nabla'_1, \dots, \nabla'_b\}$  such that  $\frac{1}{b} \sum_{i=1}^b \nabla_i = \frac{1}{b} \nabla'_i$  but, for some gradient  $\nabla$ ,

$$(\mathbf{F}_{\mathcal{G}} + \epsilon \mathbf{I})^{-1} \nabla \neq (\mathbf{F}_{\mathcal{G}} + \epsilon \mathbf{I})^{-1} \nabla'. \quad (55)$$

We now construct such  $\mathcal{B}$  and  $\mathcal{B}'$ , but emphasize that this is only one of many possible ways to construct such an example. First, take  $\mathcal{D}_n = \{(\mathbf{x}_1, \mathbf{y}_1), \dots, (\mathbf{x}_n, \mathbf{y}_n)\}$  such that  $\{\mathbf{x}_i\}_{i=1}^n$  is an orthonormal basis, meaning  $\mathbf{x}_i^{\top} \mathbf{x}_j = \delta_{i,j}$ . This means that FIM is the identity

$$\mathbf{F}_{\mathcal{G}} = \frac{1}{n} \sum_{i=1}^n \mathbf{x}_i \mathbf{x}_i^{\top} = \mathbf{I}. \quad (56)$$

Thus,

$$(\mathbf{F}_{\mathcal{G}} + \epsilon \mathbf{I})^{-1} = \text{diag}((1 + \epsilon)^{-1}, \dots, (1 + \epsilon)^{-1}). \quad (57)$$

Now, define  $\mathcal{D}'_n = \{(\mathbf{x}'_1, \mathbf{y}'_1), \dots, (\mathbf{x}'_n, \mathbf{y}'_n)\}_{i=1}^b$  such that  $\mathbf{x}'_1 = 2\mathbf{x}_1, \dots, \mathbf{x}'_n = 2\mathbf{x}_n$ . The FIM in this case is

$$\mathbf{F}_{\mathcal{G}'} = 4\mathbf{I} \quad (58)$$

and

$$(\mathbf{F}_{\mathcal{G}'} + \epsilon \mathbf{I})^{-1} = \text{diag}((4 + \epsilon)^{-1}, \dots, (4 + \epsilon)^{-1}). \quad (59)$$

Therefore, for any non-zero gradient  $\nabla$  we have

$$\Phi_{\text{nat}}(\nabla, \mathcal{G}) = (\mathbf{F}_{\mathcal{G}} + \epsilon)^{-1} \nabla = (1 + \epsilon)^{-1} \nabla \neq (4 + \epsilon)^{-1} \nabla = (\mathbf{F}_{\mathcal{G}'} + \epsilon)^{-1} \nabla = \Phi_{\text{nat}}(\nabla, \mathcal{G}'). \quad (60)$$

This proves  $\Phi_{\text{nat}}$  non-trivially depends on the FIM. To see that  $\Phi_{\text{OBD}}$  and  $\Phi_{\text{OBS}}$  non-trivially depends on the FIM, take  $\mathcal{D}_n$  and  $\mathcal{D}'_n$  as before, and choose any non-zero  $\theta$ .

□

The next proposition now follows from Propositions 5 and 8.

**Proposition 9.**  *$\Phi_{\text{nat}}$ ,  $\Phi_{\text{OBD}}$ , and  $\Phi_{\text{OBS}}$  cannot be approximated (in the  $\ell_{\infty}$  sense) by continuous functions that rely only on the average gradient.*

## E.2 Universal Approximation Results

In the discussion below, we are concerned with functions from compact input domain  $\mathcal{K} \subset \Gamma_b[f]$  such that  $\mathcal{K} \cap \mathcal{E} = \emptyset$ , where

$$\mathcal{E} := \bigcup_{l=1}^{L-1} \bigcup_{i_1=1}^l \bigcup_{i_2=i_1+1}^l \left\{ \mathbf{g} \in \Gamma_b[f] \left| \sum_{j=1}^b \mathbf{g}_{i_1,j,:}^{(l)} = \sum_{j=1}^b \mathbf{g}_{i_2,j,:}^{(l)} \right. \right\} \quad (61)$$

is a finite union of linear spaces of co-dimension  $f$ . Similar assumptions over  $gK$  were used for the universality proofs in Finkelshtein et al. [23], Maron et al. [53].

For the readers convinience, we recall that for an MLP with input dimension  $d_0$ , output dimension  $d_L$ , hidden dimensions  $d_1, \dots, d_{L-1}$ , we define  $G = S_{d_1} \times \dots \times S_{d_{L-1}}$ , and  $G_b = S_b \times G$ .  $G$  acts naturally on the spaces  $\Theta[f]$  and  $\Gamma[f]$ , while  $G_b$  has natural actions on the space  $\Theta_b[f]$  and  $\Gamma_b[f]$ . See Appendix C of definitions. These actions preserve the inherent symmetries of the spaces they are defined over and so we aim to respect them through equivariance/invariance.

### Main universality proofs.

**Theorem 10.** *Let  $\mathcal{K} \subset \Gamma_b[f]$  be a compact domain such that  $\mathcal{K} = \cup_{g \in G_b} g \cdot \mathcal{K}$  and  $\mathcal{K} \cap \mathcal{E} = \emptyset$ . GradMetaNet models are universal approximators (in  $\|\cdot\|_\infty$  sense) of continuous  $G_b$ -equivariant functions from  $\mathcal{K}$  to weight space  $\Theta$ .*

*Proof.* Let  $\Phi : \mathcal{K} \rightarrow \Theta$  be a continuous  $G_b$  equivaraaint function. From proposition 13 there exists a continuous  $G_b$  equivariant function  $\Psi : \mathcal{K} \rightarrow \Gamma[f']$  and an  $G$  equivariant function  $\Lambda : \Psi(\mathcal{K}) \rightarrow \Theta$  such that  $\Phi = \Lambda \circ \Psi$ . From proposition 21 there exist a stack of layers  $L_{\text{Prod}} \circ L_\Gamma \circ \dots \circ L_\Gamma \circ \text{PE}$ <sup>4</sup> which is able to approximate  $\Lambda$  over  $\Psi(\mathcal{K})$  to any precision. Additionally, the function  $\text{PE} \circ \Psi$  is also continuous and equivariant and so, from proposition from proposition 18 there exist a stack of layers  $L_{\text{Pool}} \circ L_{\Gamma_b} \circ \dots \circ L_{\Gamma_b} \circ \text{PE}$  which is able to approximate  $\text{PE} \circ \Psi$  over  $\mathcal{K}$  to any precision. Composing the two components together allows us to construct a GradMetaNet model  $L_{\text{Prod}} \circ L_\Gamma \circ \dots \circ L_\Gamma \circ L_{\text{Pool}} \circ L_{\Gamma_b} \circ \dots \circ L_{\Gamma_b} \circ \text{PE}$  which is able to approximate  $\Phi = \Lambda \circ \Psi$  to any precision.  $\square$

As a result of Theorem 10, we obtain the following formal statement of Corollary 3.

**Corollary 11.** *Let  $\mathcal{K} \subset \Gamma_b[f]$  be a compact domain such that  $\mathcal{K} = \cup_{\tau \in G_b} \tau \cdot \mathcal{K}$  and  $\mathcal{K} \cap \mathcal{E} = \emptyset$ . there exist GradMetaNet models are able to approximate the natural gradients (see Definition 6) of elements of  $\mathcal{K}$  to arbitrary precision. Additionally, by incorporating the parameters  $\theta$  of the MLP whose gradients are provided as input to GradMetaNet into the gradient-to-weight update, GradMetaNet models are able to approximate pruning saliency scores (see Definition 7) with arbitrary precision.*

*Proof.* As was discussed in Section A.3, the natural gradients can be expressed as a function from decomposed gradient space  $\Gamma_b[3]$  to parameter space  $\Theta$ . This function is both continuous and equivariant and thus Theorem 10 shows GradMetaNet are able to approximate natural gradients. Additionally, the functions  $\Phi_1(\mathbf{g}) = \text{diag}(\mathbf{F})$  and  $\Phi_2(\mathbf{g}) = 1/\text{diag}((\mathbf{F} + \epsilon \mathbf{I})^{-1})$  are continuous equivariant functions from  $\Gamma_b$  to  $\Theta$  and thus can be approximated using GradMetaNet models. Recall that the OBD and OBD pruning saliency scores are computed by  $\Phi_1(\mathbf{g}) \odot \theta^2$  and  $\Phi_2(\mathbf{g}) \odot \theta^2$  respectively.

The parameters  $\theta = (\mathbf{W}_1, \mathbf{b}_1, \dots, \mathbf{W}_L, \mathbf{b}_L) \in \Theta$ , can be naturally added to the gradient-to-weight component  $L_{\text{Prod}}$  (See Section 5) the following way:  $L_{\text{Prod}} : \Gamma[f_{\text{in}}] \oplus \Theta \rightarrow \Theta$  applies a pointwise MLP to the feature vectors associated with the neurons connected to each weight **along with the weight of the original MLP**, or in the case of biases, to the feature vectors corresponding to the respective neuron. I.e.,  $L_{\text{Prod}}(\mathbf{g}, \theta) = (\mathbf{V}_1, \mathbf{c}_1, \dots, \mathbf{V}_L, \mathbf{c}_L)$  where

$$\mathbf{V}_{i,j}^{(l)} = \text{MLP}_1([\mathbf{g}_{i,:}^{(l)}, \mathbf{g}_{j,:}^{(l+1)}, \mathbf{W}_{i,j}^{(l)}]), \mathbf{c}_i^{(l)} = \text{MLP}_2([\mathbf{g}_{i,:}^{(l)}, \mathbf{b}_i^{(l)}]). \quad (62)$$

As we established GradMetaNet is able to approximate the functions  $\Phi_1, \Phi_2$  the update in Equation 62 can easily approximate  $\theta_{\text{OBD}} = \theta^2 \odot \Phi_1$ , and  $\theta_{\text{OBS}} = \theta^2 \odot \Phi_2$ . This completes the proof.  $\square$

<sup>4</sup>Here PE is defined for  $\Gamma[f'] = \Gamma_1[f']$ , we thus abuse notation writing PE without indicating which space it operates on.

Finally, we include a proof of universality for the invariant case

**Proposition 12.** *Let  $\mathcal{K} \subset \Gamma_b[f]$  be a compact domain such that  $\mathcal{K} = \cup_{\tau \in G_b} \tau \cdot \mathcal{K}$  and  $\mathcal{K} \cap \mathcal{E} = \emptyset$ . Invariant GradMetaNet models are universal approximators (in  $\|\cdot\|_\infty$  sense) of continuous  $G_b$ -invariant functions from  $\mathcal{K}$  to  $\mathbb{R}^d$ .*

*Proof.* Let  $\Phi : \mathcal{K} \rightarrow \mathbb{R}^d$  be a continuous  $G_b$  invariant function. From proposition 18 the gradient-bag-to-gradient component of GradMetaNet is a universal approximator of continuous equivariant functions from  $\mathcal{K}$  to  $\Gamma[d]$ . We can extend  $\Phi$  to be an equivariant function  $\tilde{\Phi} : \mathcal{K} \rightarrow \Gamma[d]$  defined by

$$\tilde{\Phi}(\mathbf{g})_{i,:}^{(l)} = \Phi(\mathbf{g}). \quad (63)$$

Since  $\Phi$  is continuous and invariant,  $\tilde{\Phi}$  is continuous and equivariant and can thus be approximated by the gradient-bag-to-gradient component of our method. Finally applying the gradient-to-vector pooling layer  $L_{\text{Vec}}$  we get that our model can approximate the function

$$\frac{1}{d_0 + \dots + d_L} \sum_{l=0}^L \sum_{i=1}^{d_l} \tilde{\Phi}(\mathbf{g})_{i,:}^{(l)} = \Phi(\mathbf{g}). \quad (64)$$

This completes the proof.  $\square$

We now prove all lemmas and propositions used in the above discussion.

### Proof of proposition 13.

**Proposition 13.** *Let  $\mathcal{K} \subset \Gamma_b[f]$  be a compact domain such that  $\mathcal{K} = \cup_{\tau \in G_b} \tau \cdot \mathcal{K}$  and  $\mathcal{K} \cap \mathcal{E} = \emptyset$  and let  $\Phi : K \rightarrow \Theta$  be a continuous  $G_b$ -equivariant function (here the  $S_b$  component of  $G_b$  acts on  $\Theta$  trivially). There exists a pair of continuous functions  $\Psi : K \rightarrow \Gamma[f']$ ,  $\Lambda : \Psi(K) \rightarrow \Theta$  such that:*

- $\Psi$  is continuous and  $G_b$ -equivariant.
- $\Lambda$  is continuous and  $G$ -equivariant.
- $\Phi = \Psi \circ \Lambda$ .

*Proof.* First, Lemma 15 states that there exists a continuous and  $G_b$ -equivariant function  $\Psi : \mathcal{E}^c \rightarrow \Gamma[f']$  (where  $\mathcal{E}^c = \{\mathbf{g} \in \Gamma_b[f] \mid \mathbf{g} \notin \mathcal{E}\}$ ), such that for every  $\mathbf{g}_1, \mathbf{g}_2 \in \mathcal{E}^c$

$$\Psi(\mathbf{g}_1) = \Psi(\mathbf{g}_2) \iff \exists \tau \in S_b \text{ s.t. } \mathbf{g}_1 = \tau \cdot \mathbf{g}_2. \quad (65)$$

Now let  $\pi : \Gamma_b[f] \rightarrow \Gamma_b[f]/S_b$  be the projection map to the quotient space induced by the orbits of  $S_b$ . Note that the group  $G$  acts naturally on the quotient space  $\Gamma_b[f]/S_b$  by:

$$\tau \cdot \{\sigma \cdot \mathbf{g} \mid \sigma \in S_b\} = \{\tau \cdot \sigma \cdot \mathbf{g} \mid \sigma \in S_b\}. \quad (66)$$

Additionally, as the set  $K$  is compact, the set  $\tilde{\mathcal{K}} = \pi(\mathcal{K})$  is also compact. Since  $\Phi, \Psi$  are invariant to the action of  $S_b$  and equivariant to  $G$ , Lemma 16 implies that there exist continuous  $G$ -equivariant functions  $\tilde{\Psi} : \tilde{\mathcal{K}} \rightarrow \Gamma[f']$ ,  $\tilde{\Phi} : \tilde{\mathcal{K}} \rightarrow \Theta$  such that  $\Psi = \tilde{\Psi} \circ \pi$  and  $\Phi = \tilde{\Phi} \circ \pi$ . As  $\Psi$  is  $S_b$ -injective, the function  $\tilde{\Psi}$  is injective and thus the function  $\tilde{\Psi}^{-1} : \Psi(\mathcal{K}) \rightarrow \tilde{\mathcal{K}}$  is well defined. Additionally, as  $\tilde{\Psi}$  is  $G$  equivariant  $\tilde{\Psi}^{-1}$  is also  $G$  equivariant. We now define  $\Lambda = \tilde{\Phi} \circ \tilde{\Psi}^{-1} : \Psi(\mathcal{K}) \rightarrow \Theta$ . Since  $\tilde{\Phi}$  and  $\tilde{\Psi}^{-1}$  are  $G$ -equivariant,  $\Lambda$  is  $G$ -equivariant. Additionally,

$$\Lambda \circ \Psi = \tilde{\Phi} \circ \tilde{\Psi}^{-1} \circ \Psi = \tilde{\Phi} \circ \tilde{\Psi}^{-1} \circ \tilde{\Psi} \circ \pi = \tilde{\Phi} \circ \pi = \Phi. \quad (67)$$

Finally, by Lemma 17  $\Lambda$  is continuous, completing the proof.  $\square$

We now state and prove all the lemmas used in the proof of proposition 13, starting with Lemma 3 from [53] restated below:

**Lemma 14.** *Let  $H < S_n$  act on  $\mathbb{R}^{n \times f}$  by applying the same element  $\tau \in H$  to each channel, then there exists a polynomial function  $U : \mathbb{R}^{n \times f} \rightarrow \mathbb{R}^{f'}$  for some  $f' \in \mathbb{N}$  for which  $U(\mathbf{x}) = U(\mathbf{y})$  if and only if  $\mathbf{x} = \tau \cdot \mathbf{y}$  for some  $\tau \in H$ .*

**Lemma 15.** *There exists a continuous  $G_b$ -equivariant function  $\Psi : \mathcal{E}^c \rightarrow \Gamma[f']$  such that for every  $\mathbf{g}_1, \mathbf{g}_2 \in \mathcal{E}^c$*

$$\Psi(\mathbf{g}_1) = \Psi(\mathbf{g}_2) \iff \exists \tau \in S_b \text{ s.t. } \mathbf{g}_1 = \tau \cdot \mathbf{g}_2. \quad (68)$$

*Proof.* Let  $U$  be the polynomial invariant function established in Lemma 14 where  $H = G_b$ , and define  $S : \mathcal{E}^c \rightarrow \Gamma[f]$  by

$$S(\mathbf{g})_{i,:}^{(l)} = \sum_{j=1}^b \mathbf{g}_{j,i,:}^{(l)} \quad (69)$$

We now define  $\Psi : \mathcal{E}^c \rightarrow \Gamma[f']$  by:

$$\Psi(\mathbf{g})_{i,:}^{(l)} = [S^{(l)}(\mathbf{g})_{i,:}, U(\mathbf{g})] \quad (70)$$

where  $[\dots]$  represents concatenation along the feature dimension. Note that we slightly abuse the notation of the feature dimension, denoting it as  $f'$  multiple times. We first notice that since  $S$  is equivariant and continuous and  $U$  is invariant and continuous,  $\Psi$  is also equivariant and continuous. Now, for input vectors  $\mathbf{g}_1, \mathbf{g}_2 \in \mathcal{E}^c$  if there exists a group element  $\tau \in S_b$  such that  $\mathbf{g}_1 = \tau \cdot \mathbf{g}_2$  then from equivariance we have  $\Psi(\mathbf{g}_1) = \Psi(\tau \cdot \mathbf{g}_2) = \tau \cdot \Psi(\mathbf{g}_2) = \Psi(\mathbf{g}_2)$  where the last inequality holds as  $S_b$  acts trivially on the output space  $\Gamma[f]$ . On the other hand, assume  $\Psi(\mathbf{g}_1) = \Psi(\mathbf{g}_2)$ . We consider 2 cases:

**Case 1:** for every  $\tau_1, \tau_2 \in G_b = S_b \times G$  it holds that  $\tau_1 \cdot \tau_2 \cdot \mathbf{g}_2 \neq \mathbf{g}_1$ . In this case from the definition of  $U$  it holds that  $U(\mathbf{g}_1) \neq U(\mathbf{g}_2)$  and so  $\Psi(\mathbf{g}_1) \neq \Psi(\mathbf{g}_2)$ .

**Case 2:** There exist a pair  $\tau_1, \tau_2 \in G_b = S_b \times G$  such that  $\tau_1 \cdot \tau_2 \cdot \mathbf{g}_2 = \mathbf{g}_1$ . Assume by contradiction that  $\tau_2$  is not the identity. Recall that for every  $\mathbf{g} \notin \mathcal{E}$ ,  $l \in [L]$ ,  $i \neq j \in [d_l]$ , it holds that

$$\sum_{k=1}^b \mathbf{g}_{k,i,:}^{(l)} \neq \sum_{k=1}^b \mathbf{g}_{k,j,:}^{(l)} \quad (71)$$

Thus,

$$S(\mathbf{g}_1) \neq \tau_2 \cdot S(\mathbf{g}_1) = S(\tau_2 \cdot \mathbf{g}_1) = S(\tau_1 \cdot \tau_2 \cdot \mathbf{g}_1) = S(\mathbf{g}_2). \quad (72)$$

This implies that  $\Psi(\mathbf{g}_1) \neq \Psi(\mathbf{g}_2)$ . We have thus shown that  $\Psi(\mathbf{g}_1) = \Psi(\mathbf{g}_2) \iff \exists \tau \in S_b \text{ s.t. } \mathbf{g}_1 = \tau \cdot \mathbf{g}_2$  completing the proof.  $\square$

**Lemma 16.** *Let  $\mathcal{K} \subset \Gamma_b[f]$  be a compact set such that  $\mathcal{K} = \cup_{g \in G_b} g \cdot \mathcal{K}$ . Furthermore, let  $\Phi : \mathcal{K} \rightarrow \Gamma[f']$  be a continuous  $G_b$ -equivariant function. Finally, let  $\pi : \Gamma_b[f] \rightarrow \Gamma_b[f]/S_b$  denote the projection map to the quotient space induced by the orbits of  $S_b$  and define  $\tilde{\mathcal{K}} = \pi(\mathcal{K})$ . The following holds:*

- $G$  acts on  $\Gamma_b[f]/S_b$  by  $\tau \cdot \{\sigma \cdot \mathbf{g} \mid \sigma \in S_b\} = \{\tau \cdot \sigma \cdot \mathbf{g} \mid \sigma \in S_b\}$ .
- $\pi$  is  $G$  equivariant.
- There exists a continuous  $G$ -equivariant function  $\tilde{\Phi} : \tilde{\mathcal{K}} \rightarrow \Gamma[f']$  such that  $\Phi = \tilde{\Phi} \circ \pi$ .

*Proof.* Recall that each element in  $\Gamma_b[f]/S_b$  is of the form  $\pi(\mathbf{g}) = \{\sigma \cdot \mathbf{g} \mid \sigma \in S_b\}$ . The first statement is trivial, as

$$e \cdot \{\sigma \cdot \mathbf{g} \mid \sigma \in S_b\} = \{\sigma \cdot \mathbf{g} \mid \sigma \in S_b\} \quad (73)$$

and for every  $\tau_1, \tau_2 \in G$  we have

$$(\tau_1 \cdot \tau_2) \cdot \{\sigma \cdot \mathbf{g} \mid \sigma \in S_b\} = \{\tau_1 \cdot \tau_2 \cdot \sigma \cdot \mathbf{g} \mid \sigma \in S_b\} = (\tau_1 \cdot (\tau_2 \cdot \{\sigma \cdot \mathbf{g} \mid \sigma \in S_b\})). \quad (74)$$

To prove the second statement, notice that for every  $\tau \in G$ ,  $\sigma \in S_b$ , we have  $\tau \cdot \sigma = \sigma \cdot \tau$ . Thus

$$\pi(\tau \cdot \mathbf{g}) = \{\sigma \cdot \tau \cdot \mathbf{g} \mid \sigma \in S_b\} = \{\tau \cdot \sigma \cdot \mathbf{g} \mid \sigma \in S_b\} = \tau \cdot \pi(\mathbf{g}). \quad (75)$$

Finally, to prove the last statement we recall that since  $\Phi$  is continuous and  $S_b$  invariant, from the definition of the projection map  $\pi$  there exists a continuous function  $\tilde{\Phi} : \tilde{\mathcal{K}} \rightarrow \Gamma[f']$  such that  $\Phi = \tilde{\Phi} \circ \pi$ . To show that  $\tilde{\Phi}$  is  $G$  equivariant, we notice that for every  $\tilde{\mathbf{g}} \in \tilde{\mathcal{K}}$  there exists  $\mathbf{g} \in \mathcal{K}$  such that  $\pi(\mathbf{g}) = \tilde{\mathbf{g}}$ , thus for every  $\tau \in G$

$$\tilde{\Phi}(\tau \cdot \tilde{\mathbf{g}}) = \tilde{\Phi}(\tau \cdot \pi(\mathbf{g})) = \tilde{\Phi}(\pi(\tau \cdot \mathbf{g})) = \Phi(\tau \cdot \mathbf{g}) = \tau \cdot \Phi(\mathbf{g}) = \tau \cdot \tilde{\Phi}(\pi(\mathbf{g})) = \tau \cdot \tilde{\Phi}(\tilde{\mathbf{g}}) \quad (76)$$

and so  $\tilde{\Phi}$  is equivariant, completing the proof.  $\square$

**Lemma 17.** *Let  $\mathcal{K} \subset \mathbb{R}^f$  be a compact domain and  $\Phi : \mathcal{K} \rightarrow \mathbb{R}^{f'}$  be a continuous function such that  $\Phi = \Lambda \circ \Psi$ . If  $\Psi$  is continuous, then  $\Lambda$  is continuous on  $\Psi(\mathcal{K})$ .*

The proof of this lemma is identical to that of Lemma 5 from [53], still we provide a proof below.

*Proof.* Assume that this is incorrect, then there is a sequence  $\mathbf{y}_i = \Psi(\mathbf{x}_i)$  such that  $\mathbf{y}_i \rightarrow \mathbf{y}_0$  but  $\Lambda(\mathbf{y}_i) \not\rightarrow \Lambda(\mathbf{y}_0)$ . Without loss of generality, assume that  $\mathbf{x}_i \rightarrow \mathbf{x}_0 \in \mathcal{K}$  (otherwise choose a converging sub sequence). We have

$$\Phi(\mathbf{x}_i) = \Lambda(\Psi(\mathbf{x}_i)) = \Lambda(\mathbf{y}_i) \not\rightarrow \Lambda(\mathbf{y}_0) = \Lambda(\Psi(\mathbf{x}_0)) = \Phi(\mathbf{x}_0) \quad (77)$$

which is a contradiction to the continuity of  $\Phi$ .  $\square$

### Proof of proposition 18.

**Proposition 18.**  *$\mathcal{K} \subset \Gamma_b[f]$  be a compact domain such that  $\mathcal{K} = \cup_{g \in G_b} g \cdot \mathcal{K}$  and  $\mathcal{K} \cap \mathcal{E} = \emptyset$ , and let  $\Phi : \mathcal{K} \rightarrow \Gamma[f']$  be a continuous  $G_b$ -equivariant function. For every  $\epsilon > 0$  There exists a stack of layers  $\mathbf{F} = L_{\text{Pool}} \circ L_{\Gamma_b} \circ \dots \circ L_{\Gamma_b} \circ \text{PE}$  (As defined in Section 5)  $\mathbf{F}^{\text{GradMetaNet}}$  such that for every  $\mathbf{g} \in \mathcal{K}$ :*

$$\|\Phi(\mathbf{g}) - \mathbf{F}(\mathbf{g})\| < \epsilon. \quad (78)$$

*Proof.* From Lemma 19, there exists a continuous  $S_b \times S_{d_0+\dots+d_L}$ -equivariant function  $\Psi : \Gamma_b[f+k] \rightarrow \Gamma[f']$  such that  $\Phi = \Psi \circ \text{PE}$ . As  $\Psi$  is continuous and  $S_b \times S_{d_0+\dots+d_L}$ -equivariant, it was shown e.g. in Finkelshtein et al. [23], Maron et al. [53] that for each  $\epsilon > 0$  there exists a Deep Symmetric Sets network for sets of sets of the form  $\tilde{\mathbf{F}} = L_{\text{Pool}} \circ L_{\Gamma_b} \circ \dots \circ L_{\Gamma_b}$  such that for every  $\mathbf{g} \in \text{PE}(\mathcal{K})$ :

$$\|\Psi(\mathbf{g}) - \tilde{\mathbf{F}}(\mathbf{g})\| < \epsilon. \quad (79)$$

This implies for every  $\mathbf{g} \in \mathcal{K}$ :

$$\|\Phi(\mathbf{g}) - \mathbf{F}(\mathbf{g})\| = \|\Psi(\text{PE}(\mathbf{g})) - \tilde{\mathbf{F}}(\text{PE}(\mathbf{g}))\| < \epsilon \quad (80)$$

Completing the proof.  $\square$

**Lemma 19.** *Let  $\Phi : \Gamma_b[f] \rightarrow \Gamma[f']$  be a continuous  $G_b$  equivariant function and let  $\text{PE} : \Gamma_b[f] \rightarrow \Gamma_b[f+k]$  be a positional encoding layer as defined in Section 5. there exists an  $S_n \times S_{d_0+\dots+d_L}$  equivariant function  $\Psi : \Gamma_b[f+k] \rightarrow \Gamma[f']$  such that  $\Phi = \Psi \circ \text{PE}$ .*

*Proof.* As  $\text{PE}$  is injective we can define  $\Lambda : \text{PE}(\Gamma_b[f]) \rightarrow \Gamma[f']$  by  $\Lambda(\mathbf{g}) = \Phi(\text{PE}^{-1}(\mathbf{g}))$ . We now extend  $\Lambda$  to the domain  $\cup_{\sigma \in S_{d_0+\dots+d_L}} \sigma \cdot \text{PE}(\Gamma_b[f])$  by defining for every  $\mathbf{g} \in \text{PE}(\Gamma_b[f])$ ,  $\sigma \in S_{d_0+\dots+d_L}$ ,  $\Lambda(\sigma \cdot \mathbf{g}) = \sigma \cdot \Lambda(\mathbf{g})$ . We show this extension is well defined (i.e. that there is no case where  $\sigma_1 \cdot \mathbf{g} = \sigma_2 \cdot \mathbf{g}$  but  $\sigma_1 \cdot \Lambda(\mathbf{g}) \neq \sigma_2 \cdot \Lambda(\mathbf{g})$ ). Let  $\mathbf{g}' \in \Gamma_b[f]$ ,  $\mathbf{g} = \text{PE}(\mathbf{g}')$  and  $\sigma_1 \neq \sigma_2 \in S_{d_0+\dots+d_L}$  such that  $\sigma_1 \cdot \mathbf{g} = \sigma_2 \cdot \mathbf{g}$ . It follows that  $\sigma_2^{-1} \cdot \sigma_1 \cdot \mathbf{g} = \mathbf{g}$ , and thus from the definition of the positional encoding map  $\text{PE}$ ,  $\sigma_2^{-1} \cdot \sigma_1 \in G$  and  $\sigma_2^{-1} \cdot \sigma_1 \cdot \mathbf{g}' = \mathbf{g}'$ . Thus, since  $\Phi$  is  $G$ -equivariant it holds that

$$\Lambda(\sigma_1 \cdot \mathbf{g}) = \sigma_1 \cdot \Lambda(\mathbf{g}) = \sigma_2 \cdot \sigma_2^{-1} \cdot \sigma_1 \cdot \Phi(\mathbf{g}') = \sigma_2 \cdot \Phi(\sigma_2^{-1} \cdot \sigma_1 \cdot \mathbf{g}') = \sigma_2 \cdot \Phi(\mathbf{g}') = \sigma_2 \cdot \Lambda(\mathbf{g}) = \Lambda(\sigma_2 \cdot \mathbf{g}). \quad (81)$$

Thus, the extension of  $\Lambda$  is well defined. Since the functions  $\Phi, \text{PE}$  are continuous the function  $\Lambda$  is continuous and thus there exists a continuous function  $\tilde{\Lambda} : \Gamma_b[f] \rightarrow \Gamma[f']$  such that for every  $\mathbf{g} \in \cup_{\sigma \in S_{d_0+\dots+d_L}} \sigma \cdot \text{PE}(\Gamma_b[f])$  it holds that  $\tilde{\Lambda}(\mathbf{g}) = \Lambda(\mathbf{g})$ . We define  $\Psi : \Gamma_b[f] \rightarrow \Gamma[f']$  by

$$\Psi(\mathbf{g}) = \sum_{\substack{\sigma \in S_{d_0+\dots+d_L} \\ \tau \in S_b}} \tau^{-1} \cdot \sigma^{-1} \cdot \tilde{\Lambda}(\tau \cdot \sigma \cdot \mathbf{g}). \quad (82)$$

First,  $\Psi$  is continuous and equivariant w.r.t  $S_b \times S_{d_0+\dots+d_L}$ . Second, for every  $\mathbf{g} \in \text{PE}(\Gamma_b[f])$  it holds that

$$\Psi(\mathbf{g}) = \sum_{\substack{\sigma \in S_{d_0+\dots+d_L} \\ \tau \in S_b}} \tau^{-1} \cdot \sigma^{-1} \cdot \Lambda(\tau \cdot \sigma \cdot \mathbf{g}) = \sum_{\substack{\sigma \in S_{d_0+\dots+d_L} \\ \tau \in S_b}} \tau^{-1} \cdot \sigma^{-1} \cdot \tau \cdot \sigma \cdot \Lambda(\mathbf{g}) = \Lambda(\mathbf{g}). \quad (83)$$

Thus, for every  $\mathbf{g}' \in \Gamma_b[f]$  it holds that  $\Phi(\mathbf{g}') = \Phi(\text{PE}^{-1}(\text{PE}(\mathbf{g}))) = \Psi(\text{PE}(\mathbf{g}'))$  and so  $\Phi = \Psi \circ \text{PE}$ .  $\square$

**Proof of proposition 21.** In this section we aim to leverage the universality result of the Set2Graph architecture presented in Serviansky et al. [75] to complete the universality proof of GradMetaNet. To this aim, we first define the square gradient space  $\tilde{\Gamma}[f]$ . Intuitively, the spaces  $\Gamma[f]$  and  $\tilde{\Gamma}[f]$  parallel set space and graph space, and  $\Theta[f]$  can be embedded in  $\tilde{\Gamma}[f]$ . We now formally define  $\tilde{\Gamma}[f]$ .

**Definition 20.** Square gradient space  $\tilde{\Gamma}[f]$  is defined by

$$\tilde{\Gamma}[f] = (\Gamma \otimes \Gamma)^f. \quad (84)$$

Here,  $\otimes$  denotes the tensor product, while  $^f$  represents the Cartesian power product. Thus, an element  $\tilde{\mathbf{g}} \in \tilde{\Gamma}[f]$  is of the form

$$\tilde{\mathbf{g}} = \{\tilde{\mathbf{g}}_{i,j,:}^{(l_1, l_2)}\}_{l_1, l_2 \in [L]}, \quad (85)$$

where  $i \in [d_{l_1}]$ ,  $j \in [d_{l_2}]$  and  $\tilde{\mathbf{g}}_{i,j,:}^{(l_1, l_2)} \in \mathbb{R}^f$ . The space  $\Theta[f]$  can be naturally embedded into  $\tilde{\Gamma}[2f]$  by the map  $L_{\text{ode}}$  defined below for  $\theta \in \Theta[f]$ ,  $\theta = (\mathbf{W}^{(1)}, \mathbf{b}^{(1)}, \dots, \mathbf{W}^{(L)}, \mathbf{b}^{(L)})$

$$L_{\text{ode}}(\theta)_{i,j,:}^{(l_1, l_2)} = \begin{cases} [\mathbf{W}_{i,j,:}^{(l_2)}, \mathbf{b}_{j,:}^{(l_2)}] & l_1 = l_2 + 1 \\ 0 & \text{otherwise.} \end{cases} \quad (86)$$

Additionally, the map  $L_{\text{odp}} : \tilde{\Gamma}[2f] \rightarrow \Theta[f]$  projects the space  $\tilde{\Gamma}[2f]$  to  $\Theta[f]$  and is defined by  $L_{\text{odp}}(\tilde{\mathbf{g}}) = (\mathbf{W}^{(1)}, \mathbf{b}^{(1)}, \dots, \mathbf{W}^{(L)}, \mathbf{b}^{(L)})$

$$\mathbf{W}_{i,j,:}^{(l)} = \tilde{\mathbf{g}}_{i,j,:}^{(l-1, l)}, \quad \mathbf{b}_{i,:}^{(l)} = \tilde{\mathbf{g}}_{i,i,:}^{(l-1, l)}. \quad (87)$$

The action of the group  $G = S_{d_1} \times \dots \times S_{d_{L-1}}$  on  $\Gamma[f]$  extend naturally to  $\tilde{\Gamma}[f]$  and is defined for  $\tau = (\tau_1, \dots, \tau_{L-1}) \in G$ ,  $\mathbf{g} \in \tilde{\Gamma}[f]$  by

$$(\tau \cdot \mathbf{g})_{i,j,:}^{(l_1, l_2)} = \mathbf{g}_{\tau_{l_1}^{-1}(i), \tau_{l_2}^{-1}(j), :}^{(l_1, l_2)}. \quad (88)$$

It is easy to verify that the maps  $L_{\text{ode}}, L_{\text{odp}}$  are  $G$ -equivariant.

Before stating the following proposition, we note that the positional encoding map  $\text{PE} : \Gamma_b[f] \rightarrow \Gamma_b[f+k]$  can be considered as well defined on the space  $\Gamma_b[f] = \Gamma_1[f]$  as well.

**Proposition 21.** Let  $\mathcal{K} \subset \Gamma[f]$  be a compact set such that  $\mathcal{K} = \bigcup_{g \in G} g \cdot \mathcal{K}$ , and let  $\Phi : \mathcal{K} \rightarrow \Theta[f']$  be a continuous  $G$ -equivariant function. For every  $\epsilon > 0$  There exists a stack of gradient-to-gradient layers composed with a gradient-to-weight layer and a positional encoding layer  $\mathbf{F} = L_{\text{Prod}} \circ L_{\Gamma} \circ \dots \circ L_{\Gamma} \circ \text{PE}$  such that for every  $\mathbf{g} \in K$ :

$$\|\Phi(\mathbf{g}) - \mathbf{F}(\mathbf{g})\| < \epsilon. \quad (89)$$

*Proof.* First, notice that the model  $\mathbf{F}$  is equal to  $L_{\text{odp}} \circ \bar{\mathbf{F}} \circ \text{PE}$  where  $\bar{\mathbf{F}}$  is exactly a Set2Graph architecture, from the space  $\Gamma[f]$  to  $\tilde{\Gamma}[f']$  which is equivariant to the action of the group  $S_{d_0 + \dots + d_L}$  on both spaces. This is because the deep set component in Set2Graph is identical to a stack of  $L_{\Gamma}$  layers and the broadcast and pointwise mlp components of Set2Graph are identical to the  $L_{\text{Prod}}$  component composed with the embedding  $L_{\text{ode}}$ . From Lemma 22, there exists a continuous  $S_{d_0 + \dots + d_L}$  equivariant function  $\Psi : \Gamma[f+k] \rightarrow \Theta[2f']$  such that  $\Phi = L_{\text{odp}} \circ \Psi \circ \text{PE}$ . Finally, it was shown in [75] that there exists a Set2Graph network  $\bar{\mathbf{F}}$  such that for every  $\mathbf{g} \in \text{PE}(K)$ :

$$\|\Psi(\mathbf{g}) - \bar{\mathbf{F}}(\mathbf{g})\| < \epsilon. \quad (90)$$

This implies for every  $\mathbf{g} \in K$  there exists a gradient to weight model  $\mathbf{F}$  such that :

$$\|\Phi(\mathbf{g}) - \mathbf{F}(\mathbf{g})\| = \|L_{\text{ode}}(\Psi(\text{PE}(\mathbf{g}))) - L_{\text{ode}}(\bar{\mathbf{F}}(\text{PE}(\mathbf{g})))\| < \epsilon. \quad (91)$$

This completes the proof.  $\square$

**Lemma 22.** Let  $\Phi : \Gamma[f] \rightarrow \Theta[f']$  be a continuous  $G_b$  equivariant function. There exists an  $S_b \times S_{d_0 + \dots + d_L}$  equivariant function  $\Psi : \Gamma[f+k] \rightarrow \tilde{\Gamma}[2f']$  such that  $\Phi = L_{\text{odp}} \circ \Psi \circ \text{PE}$ .

*Proof.* The proof is very similar to that of Lemma 19. Let  $\bar{\Phi} : \Gamma[f] \rightarrow \tilde{\Gamma}[2f']$  be defined by  $\bar{\Phi} = L_{\text{ode}} \circ \Phi$  and note that since  $\Phi$  and  $L_{\text{ode}}$  are continuous and  $G$  equivariant,  $\bar{\Phi}$  is also continuous and

$G$  equivariant. As PE is injective we can define  $\Lambda : \text{PE}(\Gamma[f]) \rightarrow \tilde{\Gamma}[2f']$  by  $\Lambda(\mathbf{g}) = \bar{\Phi}(\text{PE}^{-1}(\mathbf{g}))$ . We now extend  $\Lambda$  to the domain  $\cup_{\sigma \in S_{d_0+...+d_L}} \sigma \cdot \text{PE}(\Gamma[f])$  by defining for every  $\mathbf{g} \in \text{PE}(\Gamma[f])$ ,  $\sigma \in S_{d_0+...+d_L}$ ,  $\Lambda(\sigma \cdot \mathbf{g}) = \sigma \cdot \Lambda(\mathbf{g})$ . We show this extension is well defined (i.e. that there is no case where  $\sigma_1 \cdot \mathbf{g} = \sigma_2 \cdot \mathbf{g}$  but  $\sigma_1 \cdot \Lambda(\mathbf{g}) \neq \sigma_2 \cdot \Lambda(\mathbf{g})$ ).

Let  $\mathbf{g}' \in \Gamma[f]$ ,  $\mathbf{g} = \text{PE}(\mathbf{g}')$  and  $\sigma_1 \neq \sigma_2 \in S_{d_0+...+d_L}$  such that  $\sigma_1 \cdot \mathbf{g} = \sigma_2 \cdot \mathbf{g}$ . It follows that  $\sigma_2^{-1} \cdot \sigma_1 \cdot \mathbf{g} = \mathbf{g}$ , and thus from the definition of the positional encoding function PE,  $\sigma_2^{-1} \cdot \sigma_1 \in G$  and  $\sigma_2^{-1} \cdot \sigma_1 \cdot \mathbf{g}' = \mathbf{g}'$ . Thus, since  $\bar{\Phi}$  is  $G$  equivariant it holds that

$$\Lambda(\sigma_1 \cdot \mathbf{g}) = \sigma_1 \cdot \Lambda(\mathbf{g}) = \sigma_2 \cdot \sigma_2^{-1} \cdot \sigma_1 \cdot \bar{\Phi}(\mathbf{g}') = \sigma_2 \cdot \bar{\Phi}(\sigma_2^{-1} \cdot \sigma_1 \cdot \mathbf{g}') = \sigma_2 \cdot \bar{\Phi}(\mathbf{g}') = \sigma_2 \cdot \Lambda(\mathbf{g}) = \Lambda(\sigma_2 \cdot \mathbf{g}). \quad (92)$$

Thus, the extension of  $\Lambda$  is well defined. Since the functions  $\bar{\Phi}$ , PE are continuous the function  $\Lambda$  is continuous and thus there exists a continuous function  $\tilde{\Lambda} : \Gamma[f] \rightarrow \tilde{\Gamma}[2f']$  such that for every  $\mathbf{g} \in \cup_{\sigma \in S_{d_0+...+d_L}} \sigma \cdot \text{PE}(\Gamma[f])$  it holds that  $\tilde{\Lambda}(\mathbf{g}) = \Lambda(\mathbf{g})$ . We define  $\Psi : \Gamma[f] \rightarrow \tilde{\Gamma}[2f']$  by

$$\Psi(\mathbf{g}) = \sum_{\substack{\sigma \in S_{d_0+...+d_L} \\ \tau \in S_b}} \tau^{-1} \cdot \sigma^{-1} \cdot \tilde{\Lambda}(\tau \cdot \sigma \cdot \mathbf{g}). \quad (93)$$

First,  $\Psi$  is continuous and equivariant w.r.t  $S_b \times S_{d_0+...+d_L}$ . Second, for every  $\mathbf{g} \in \text{PE}(\Gamma[f])$  it holds that

$$\Psi(\mathbf{g}) = \sum_{\substack{\sigma \in S_{d_0+...+d_L} \\ \tau \in S_b}} \tau^{-1} \cdot \sigma^{-1} \cdot \Lambda(\tau \cdot \sigma \cdot \mathbf{g}) = \sum_{\substack{\sigma \in S_{d_0+...+d_L} \\ \tau \in S_b}} \tau^{-1} \cdot \sigma^{-1} \cdot \tau \cdot \sigma \cdot \Lambda(\mathbf{g}) = \Lambda(\mathbf{g}). \quad (94)$$

Thus, for every  $\mathbf{g}' \in \Gamma[f]$  it holds that

$$\bar{\Phi}(\mathbf{g}') = \bar{\Phi}(\text{PE}^{-1}(\text{PE}(\mathbf{g}'))) = \Psi(\text{PE}(\mathbf{g}')). \quad (95)$$

Finally, since  $L_{\text{odp}} \circ L_{\text{ode}} = \text{id}$  we have

$$\Phi = L_{\text{odp}} \circ \bar{\Phi} = L_{\text{odp}} \circ \Psi \circ \text{PE} \quad (96)$$

completing the proof.  $\square$

### E.3 Importance of $\mathcal{E}$ in Universality

Recall that Theorem 2 proves the universality of GradMetaNet over compact domains which do not intersect the set  $\mathcal{E} \subset \Gamma_b[f]$  defined by:

$$\mathcal{E} = \bigcup_{l=1}^{L-1} \bigcup_{i_1=1}^l \bigcup_{i_2=i_1+1}^l \left\{ \mathbf{g} \in \Gamma_b[f] \left| \sum_{j=1}^b \mathbf{g}_{i_1,j,:}^{(l)} = \sum_{j=1}^b \mathbf{g}_{i_2,j,:}^{(l)} \right. \right\} \quad (97)$$

In this section, we prove that there exist compact sets  $\mathcal{K} \subset \Gamma_b[f]$  with  $\mathcal{K} \cap \mathcal{E} \neq \emptyset$  over which GradMetaNet is not universal. We emphasize that, as discussed below, sets intersecting  $\mathcal{E}$  consist of highly regular gradient values, which deviate significantly from typical gradient sets. Consequently, the requirement  $\mathcal{K} \cap \mathcal{E} = \emptyset$  is a mild and realistic assumption.

**Proposition 23.** *There exist a pair of elements  $\mathbf{g}_1, \mathbf{g}_2 \in \mathcal{E}$  such that for any  $\tau \in G_b$ ,  $\tau \cdot \mathbf{g}_1 \neq \mathbf{g}_2$  but for every GradMetaNet model  $\mathbf{F}$  it holds that  $\mathbf{F}(\mathbf{g}_1) = \mathbf{F}(\mathbf{g}_2)$ .*

*Proof.* For simplicity, we focus in this proof on the invariant version of GradMetaNet,  $\mathbf{F} : \Gamma_b[f] \rightarrow \mathbb{R}^{f'}$ . The proof can be easily extended to the equivariant version of GradMetaNet,  $\mathbf{F} : \Gamma_b[f] \rightarrow \Theta[f']$ . Let the underlying MLP used to define the spaces  $\Gamma_b[f]$  have an input dimension  $d_0 = 1$ , a single hidden layer of dimension  $d_1 = n$ , and an output dimension  $d_2 = 1$ . In this case,  $\Gamma_b[f]$ , along with the action of  $G_b$ , is isomorphic to the space of “sets of sets” defined in Hartford et al. [31]. Moreover, GradMetaNet is equivalent to the architecture proposed in Hartford et al. [31]. This architecture is known to be unable to distinguish between certain highly regular, non-equivalent inputs. For example, incidence matrices of graphs can be viewed as sets of sets and, therefore, as elements of  $\Gamma_b[f]$ . It was shown in Albooyeh et al. [2] that the ability of the architecture in Hartford et al. [31], and consequently GradMetaNet, to separate graphs based on their incidence matrices is equivalent to the 1-WL test [88].

Consider an example where  $\mathbf{g}_1$  represents the incidence matrix of a graph consisting of two disconnected cycles of length 3, and  $\mathbf{g}_2$  represents the incidence matrix of a single cycle of length 6. For

any GradMetaNet model  $\mathbf{F}$ , it will hold that  $\mathbf{F}(\mathbf{g}_1) = \mathbf{F}(\mathbf{g}_2)$ . A straightforward check shows that for this example,  $\mathbf{g}_1, \mathbf{g}_2 \in \mathcal{E}$ , completing the proof.  $\square$

## F Experimental Details

In this section we provide all experimental details for all experiments in Section 7. We run all the experiments on a singel NVIDIA-A100-SXM4 GPU with 40GB of memory.

### F.1 Curvature Information Estimation

**Dataset.** To construct the dataset for this experiment, we first generate 3000 SIREN models [77], commonly used for INRs. Each model has three layers with 32 hidden features, i.e.  $1 \rightarrow 32 \rightarrow 32 \rightarrow 1$ . The weights and biases of these models are randomly initialized using a standard Gaussian distribution. Each data point in the resulting dataset corresponds to a single SIREN model and consists of an input gradient set of size 128,  $\mathbf{g} \in \Gamma_{128}[2]$ , and a target vector,  $\theta_{\text{FIM}} \in \Theta$ . The input gradient set corresponding to a SIREN model  $\mathbf{f}_{\theta}$  is computed by sampling 128 random points  $S_{\mathbf{f}_{\theta}} = \{x_1, \dots, x_{128}\} \subset [-1, 1]$ . To simulate diverse datasets, the points in  $S_{\mathbf{f}_{\theta}}$  are sampled from a distribution  $X_p$  defined by

$$X_p = \begin{cases} \text{U}([0, 1]), & \text{with probability } p, \\ \text{U}([-1, 0]), & \text{with probability } 1 - p. \end{cases} \quad (98)$$

Here the value of  $p$  is randomly and uniformly selected over the unit interval. The set of input gradients is then given by  $\{\nabla_1, \dots, \nabla_{128}\}$ ,  $\nabla_i = \nabla \mathbf{f}_{\theta}(x_i)$ . Thus the input vector  $\mathbf{g} \in \Gamma_{128}[2]$  is given by  $[\nabla_1, \dots, \nabla_{128}]$ .

To compute the target vector  $\theta_{\text{FIM}} \in \Theta$ , we first randomly sample 1024 random points from  $X_p$   $S'_{\mathbf{f}_{\theta}} = \{x'_1, \dots, x'_{1024}\} \subset [-1, 1]$  (Note that the sets  $S_{\mathbf{f}_{\theta}}$  and  $S'_{\mathbf{f}_{\theta}}$  are independent). We then compute the true FIM (see Section A.3) by

$$\mathbf{F} = \frac{1}{1024} \sum_{i=1}^{1024} \nabla \mathbf{f}_{\theta}(x'_i) \nabla \mathbf{f}_{\theta}(x'_i)^{\top} \in \Theta \otimes \Theta \quad (99)$$

The target vector  $\theta_{\text{FIM}} \in \Theta$  is then given by  $\theta_{\text{FIM}} = \text{diag} \mathbf{F}$ . The task is then to predict  $\theta_{\text{FIM}}$  based on the gradient set vector  $\mathbf{g}$  and is trained using  $l_2$  loss. For baselines which process data in parameter space  $\Theta[f]$  (rather than gradient set space  $\Gamma_{128}[2]$ ), the gradient vector  $\mathbf{g}$  computed from gradient set  $\{\nabla_i\}$  is replaced by representing each gradient in parameter space  $\nabla_i \in \Theta$ , and then either concatenating them resulting in a vector  $\theta \in \Theta[128]$  or averaging them, resulting in a vector in  $\theta \in \Theta$ .

**Baselines.** We compare GradMetaNet and GradMetaNet++ against multiple baselines.

**MLP + concat:** This baseline takes the gradient vector  $\mathbf{g}$  described above as input, flattens it, and feeds it into a standard MLP.

**Neuron Asymmetric GradMetaNet:** This variant respects the batch symmetries but not the gradient space symmetries of  $\Gamma_b[f]$ . It uses  $\mathbf{g}$  as input and applies a Deep Sets architecture, as described in Zaheer et al. [90]. Specifically, the vector feature for element  $i$  in the set is constructed as  $[\mathbf{g}_{i,:,:}^{(0)}, \dots, \mathbf{g}_{i,:,:}^{(L)}]$ .

**Batch Asymmetric GradMetaNet:** This variant closely resembles GradMetaNet but respects the gradient space symmetries while disregarding the batch symmetries of  $\Gamma_b[f]$ . It takes  $\mathbf{g}$  as input and applies a GradMetaNet model defined over  $\Gamma_1[256]$ , where the batch axis is “flattened”, resulting in a single gradient with a feature dimension of  $256 = 2 \cdot 128$ .

**Weight Space Models:** The variants “DWS+Concat”, “DWS+Average”, “GMN+Concat”, and “GMN+average” take as input the gradients represented as  $\theta \in \Theta[f]$ . Here,  $\theta$  is either the average of the gradients in the set, in which case  $f = 1$ , or the concatenation of all gradients in the set, in which case  $f = 128$ . These variants then apply either the deep weight space (DWS) architecture described in Navon et al. [61] or the graph metanetwork (GMN) architecture introduced in Lim et al. [48] to the corresponding input vector.

Table 5: Comparison of baseline properties.

Baseline	Supports sets of gradients	Supports efficient gradient representation	$S_b$ -invariant	$G$ -equivariant
MLP + Concat	✓	✓	✗	✗
DWS + Concat	✓	✓	✗	✓
GMN + Concat	✓	✓	✗	✓
DWS + Average	✗	✗	—	✓
GMN + Average	✗	✗	—	✓
Batch Asymmetric GradMetaNet	✓	✓	✗	✓
Neuron Asymmetric GradMetaNet	✓	✓	✓	✗
GradMetaNet	✓	✓	✓	✓
GradMetaNet++	✓	✓	✓	✓

**Standard Estimator:** Finally, to highlight the benefits of learning to approximate algorithms rather than relying on fixed, non-learnable approximations, we compare GradMetaNet and GradMetaNet++ to a standard estimation of the target. Specifically, we compute  $\text{diag}F_{\mathcal{B}_1}$  based on the 128 gradients provided as input and evaluate its  $\ell_2$  distance to the target, which, as a reminder, is  $\text{diag}F_{\mathcal{B}_2}$ . Here,  $\mathcal{B}_2$  is computed using the gradients of a larger set of 1024 points, independently generated from the data points in  $\mathcal{B}_1$ .

**Data preparation.** We use 500 examples as a test dataset and 500 examples as a validation dataset, with the size of the training set varying between 10 and 2000 examples. As a preprocessing step, all data, including the target vectors, is normalized based on the statistics of the training dataset. The following are the three normalization methods used, based on the vector space to which the data belongs:

1. For input vectors of the form  $\mathbf{g} \in \Gamma_{128}[2]$ : for each layer  $l = 0, \dots, 3$ , we compute the mean  $\mu^{(l)}$  and standard deviation  $\sigma^{(l)}$  over the set of values:

$$\{\mathbf{g}_{i,j,k}^{(l)} \mid i = 0, \dots, b; j = 1, \dots, d_l; k = 0, 1; \mathbf{g} \in \mathcal{D}_{\text{train}}\}.$$

We then normalize the data by:  $\mathbf{g}^{(l)} \leftarrow \frac{\mathbf{g}^{(l)} - \mu^{(l)}}{\sigma^{(l)}}$ .

2. For input vectors of the form  $\theta \in \Theta[f]$   $\theta = (\mathbf{W}^{(1)}, \mathbf{b}^{(1)}, \mathbf{W}^{(L)}, \mathbf{b}^{(L)},)$  (where  $f = 1$  for averaging or  $f = 128$  for concatenation): we follow the normalization scheme suggested in Navon et al. [60], where for each layer  $l = 1, \dots, 3$ , we compute the means  $\mu_w^{(l)}, \mu_b^{(l)}$  and standard deviations  $\sigma_w^{(l)}, \sigma_b^{(l)}$  over the sets of values:

$$\{\mathbf{W}_{i,j,k}^{(l)} \mid i = 1, \dots, d_{l-1}; j = 1, \dots, d_l; k = 0, \dots, f; \mathbf{W}^{(l)} \in \mathcal{D}_{\text{train}}\}.$$

$$\{\mathbf{b}_{i,k}^{(l)} \mid i = 1, \dots, d_l; k = 0, \dots, f; \mathbf{b}^{(l)} \in \mathcal{D}_{\text{train}}\}.$$

We then normalize the data as follows:

$$\mathbf{W}^{(l)} \leftarrow \frac{\mathbf{W}^{(l)} - \mu_w^{(l)}}{\sigma_w^{(l)}}, \quad \mathbf{b}^{(l)} \leftarrow \frac{\mathbf{b}^{(l)} - \mu_b^{(l)}}{\sigma_b^{(l)}}.$$

3. For target vectors  $\theta_{\text{FIM}} \in \Theta$ : recall that  $\Theta \cong \mathbb{R}^P$  for some integer  $P \in \mathbb{N}$ . Let  $\theta_{\text{FIM}}(i)$  denote the  $i$ -th entry of the vector  $\theta_{\text{FIM}} \in \mathbb{R}^P$ . We compute a single mean  $\mu$  and a single standard deviation  $\sigma$  over the set of values:  $\{\theta_{\text{FIM}}(i) \mid i = 1, \dots, P; \theta_{\text{FIM}} \in \mathcal{D}_{\text{train}}\}$ . The data is then normalized as:  $\theta_{\text{FIM}} \leftarrow \frac{\theta_{\text{FIM}} - \mu}{\sigma}$ .

**Additional experimental details.** Following the experimental setup in Navon et al. [60], all learned baselines in this experiment consist of approximately 15K learned parameters and roughly 3 layers (In some cases, where the input dimensionality was extremely large, it was not possible to maintain the 15K parameter budget with 3 layers). All models were trained for 100 epochs using the Adam optimizer with a learning rate of  $1 \times 10^{-3}$  and a batch size of 32. We report the test loss corresponding to the best validation performance and repeat the experiment with random seeds 1 through 5.

## F.2 Learned Optimizers

**Learned optimization tasks.** The following are descriptions of the optimization tasks the learned optimizers were evaluated on. Across all tasks, the training loss is negative log-likelihood and batch size is 128 except for the transformers task.

Table 6: Multiplicative improvement in the number of steps needed to reach Adam’s best test loss, as well as the best test loss achieved by each standard and GradMetaNet-based learned optimizer. For each task, we run Adam, record its best test loss  $L$  and the number of steps  $N$  required to reach it. We then run each learned optimizer, measure how many steps it takes to reach  $L$ , and report the improvement relative to  $N$ . The “Step Reduction Factor vs. Adam” column thus indicates a multiplicative speedup in optimization steps. The “Best Test NLL” column record the best test loss achieved by the optimizer in the run. Results are averaged across 5 optimization runs.

Dataset	Optimizer	Step Reduction Factor vs. Adam ( $\uparrow$ )	Best Test NLL ( $\downarrow$ )
F-MNIST	Adam	$1.00 \pm 0.00x$	$0.475 \pm 0.011$
	SGDM	$1.13 \pm 0.17x$	$0.463 \pm 0.019$
	DS	$1.27 \pm 0.36x$	$0.460 \pm 0.011$
	UNF	$1.16 \pm 0.18x$	$0.451 \pm 0.015$
	DS + GradMetaNet	$1.44 \pm 0.43x$	<b><math>0.445 \pm 0.017</math></b>
	UNF + GradMetaNet	<b><math>1.51 \pm 0.59x</math></b>	$0.447 \pm 0.011$
CIFAR10	Adam	$1.00 \pm 0.00x$	$1.616 \pm 0.039$
	SGDM	$1.41 \pm 0.52x$	$1.556 \pm 0.014$
	DS	$2.32 \pm 0.42x$	$1.494 \pm 0.015$
	UNF	$2.64 \pm 0.53x$	$1.516 \pm 0.020$
	DS + GradMetaNet	<b><math>4.63 \pm 1.11x</math></b>	$1.427 \pm 0.018$
	UNF + GradMetaNet	$4.26 \pm 0.56x$	<b><math>1.418 \pm 0.022</math></b>
CIFAR100	Adam	$1.00 \pm 0.00x$	$3.449 \pm 0.021$
	SGDM	$1.06 \pm 0.07x$	$3.424 \pm 0.026$
	DS	$1.79 \pm 0.40x$	$3.356 \pm 0.027$
	UNF	$1.58 \pm 0.27x$	$3.345 \pm 0.036$
	DS + GradMetaNet	<b><math>3.15 \pm 0.56x</math></b>	<b><math>3.253 \pm 0.019</math></b>
	UNF + GradMetaNet	$2.85 \pm 0.38x$	$3.262 \pm 0.013$
LM1B	Adam	$1.00 \pm 0.00x$	$6.904 \pm 0.075$
	SGDM	$1.01 \pm 0.03x$	$7.045 \pm 0.031$
	DS	$0.88 \pm 0.14x$	$6.987 \pm 0.108$
	UNF	$1.48 \pm 0.16x$	$6.702 \pm 0.080$
	DS + GradMetaNet	$1.09 \pm 0.16x$	$6.993 \pm 0.076$
	UNF + GradMetaNet	<b><math>1.82 \pm 0.39x</math></b>	<b><math>6.557 \pm 0.061</math></b>

- (1) **MLP on FashionMNIST.** Learned optimizers are tasked with training a three-layer MLP classifier on a downsized ( $8 \times 8$ ) flattened version of FashionMNIST [89]. The MLP has a single hidden layer of dimension 32 and ReLU activations.
- (2) **MLP on CIFAR10.** Learned optimizers are tasked with training a three-layer MLP classifier on a downsized ( $8 \times 8$ ) flattened version of CIFAR10. The MLP has a single hidden layer of dimension 32 and ReLU activations.
- (3) **MLP on CIFAR100.** Learned optimizers are tasked with training a three-layer MLP classifier on a downsized ( $8 \times 8$ ) flattened version of CIFAR100. The MLP has a single hidden layer of dimension 128 and ReLU activations.
- (4) **Transformer on LM1B.** Learned optimizers are tasked with training a transformer language model on LM1B [14], using next token prediction. The transformer comprises two blocks with an embedding dimension of 32, and uses four self-attention heads. We train with a batch size of 8 on length 8 sequences.
- (5) **2-parameter linear regression.** Learned optimizers are tasked with training a linear regression model with two inputs and a single output. The input training data is a mixture of two Gaussians centered around  $(1, 2)$  and  $(2, 1)$  and the target is always 0. This results in a loss landscape with non-standard curvature, as depicted in Figure 8.

**Learned optimizer architectural details.** In each inner training iteration, all learned optimizers are provided with the current parameters  $\theta_t$ , current gradient  $\nabla_t$ , six momentum values  $\{v_t^{0.1}, v_t^{0.5}, v_t^{0.9}, v_t^{0.99}, v_t^{0.999}, v_t^{0.9999}\}$ , iteration number  $t$  as an 11-dimensional sinusoidal encod-

Table 7: Training iteration speed (in iterations per second) for Adam, UNF, and UNF + GradMetaNet on LM1B (Transformer) and CIFAR100 (MLP).

Optimizer	Transformer on LM1B (It/s)	MLP on CIFAR100 (It/s)
Adam	$107.55 \pm 8.09$	$359.54 \pm 5.67$
UNF	$75.45 \pm 2.32$	$304.60 \pm 12.45$
UNF + GradMetaNet	$65.61 \pm 0.31$	$264.33 \pm 4.94$

ing. All of these inputs are concatenated across the feature dimension, to get a 19-dimensional vector per-parameter. I.e. the learned optimizers inputs are in  $\Theta[19]$  and outputs are in  $\Theta[1]$ .

For GradMetaNet based learned optimizers, inputs also include current set of individual gradients  $\mathbf{g} \in \Gamma_b$  and six momentum value  $\{\mathbf{v}_t^{0.1}, \mathbf{v}_t^{0.5}, \mathbf{v}_t^{0.9}, \mathbf{v}_t^{0.99}, \mathbf{v}_t^{0.999}, \mathbf{v}_t^{0.9999}\}$  concatenated across the feature dimension, resulting in an input in  $\Gamma_b[7]$ . These inputs are processed by GradMetaNet, that outputs an embedding in  $\Theta[14]$ , i.e. a 14-dimension embedding vector per parameter. This embedding is concatenated to the other inputs of the learned optimizer, so the DeepSets/UNF based learned optimizer gets an input in  $\Theta[33]$ .

The DeepSets [90] based learned optimizers process the inputs by applying a per-parameter MLP with three hidden layers of size 32. The UNF [91] based learned optimizers apply a per parameter MLP with two hidden layers of size 32 and output dimensions of 32, followed by a singe UNF layer. As a baseline compared against all learned optimizers we used a standard Adam optimizer [40] with learning rate tuned by grid-search over the values  $\{0.0005 * j\}_{j=1}^{20}$  (i.e. 20 equidistant values in the range  $[0.0005, 0.01]$ ).

**Meta-training details.** We meta-train for 50,000 steps using Adam [40] with learning rate  $10^{-4}$ , estimating meta-gradients over 16 parallel training runs using persistent evolutionary strategies (PES) [84] with a truncation length of 50. The meta-training objective is training loss at the end of the inner training horizon  $T$ , which is  $T = 2,000$  for image classification tasks,  $T = 5,000$  for the transformer language modeling task, and  $T = 10$  for the 2D linear regression experiment. For all methods, we initialize  $\alpha = 0.1$ ,  $\mu = 0.9$  and  $\beta = 0.001$  before meta-training. We use the learned optimizer meta-training setup from Metz et al. [57] (project available at [https://github.com/google/learned\\_optimization](https://github.com/google/learned_optimization), released under Apache License 2.0).

**Train time.** We measured the time per training iteration (in iterations per second) for Adam, UNF, and UNF + GradMetaNet on LM1B and CIFAR100. The results are reported in Table 7. All models and optimizers run on a singel NVIDIA A100-SXM4-40GB GPU. As expected, learned optimizers introduce some computational overhead. GradMetaNet incurs additional cost relative to base UNF due to processing gradient sets. However, as shown in our main results, GradMetaNet consistently converges faster than Adam—often reaching equivalent test loss in significantly fewer training steps.

**Additional results.** In Table 6 we add to Table 1 the standard deviation of the average step reduction factor for each optimizer, as well as the best test loss achieved by each optimizer in the training horizon (2,000 for image classification tasks and 5,000 for the LM task). For the reader’s convenience, in Figure 9 we presented a larger version of the plots in Figure 6

### F.3 INR Editing

**Dataset.** We utilized two previously proposed INR datasets: MNIST INRs [60] and CIFAR10 INRs [92]. Each INR represents an image from the original image datasets, and consists of three layers with 32 hidden features. The target images are produced using the image processing library OpenCV [10], by dilating or increase the contrast of the MNIST and CIFAR-10 images, respectively. To construct the input gradient set,  $\mathbf{g} \in \Gamma_{64}$ , we sample 64 random input coordinates in  $[0, 1]^2$  and compute the gradients of the editing loss w.r.t the original INR parameters. Specifically, if  $\theta$  are the INR parameters and  $\mathbf{I}_i : [0, 1]^2 \rightarrow \mathbb{R}^3$  is the target image, then for an input coordinates  $(x_i, y_i)$ , the gradient  $\nabla_i$  is given by  $\nabla_i = \nabla_{\theta} (\mathbf{f}_{\theta}(x_i, y_i) - \mathbf{I}_i(x_i, y_i))^2$ . We use the same set of random coordinates for all INRs.

**Combining GradMetaNet and weight-space methods.** We combine GradMetaNet and the weight-space architectures as follows: First, GradMetaNet processes the gradients  $\mathbf{g} \in \Gamma_{64}$  to produce outputs in  $\Theta[f]$ . In this experiment we choose  $f = 8$ . Next, the output is used as additional weight features for the weight-space network, i.e., the input to the weight-space network is in  $\Theta[9]$ .

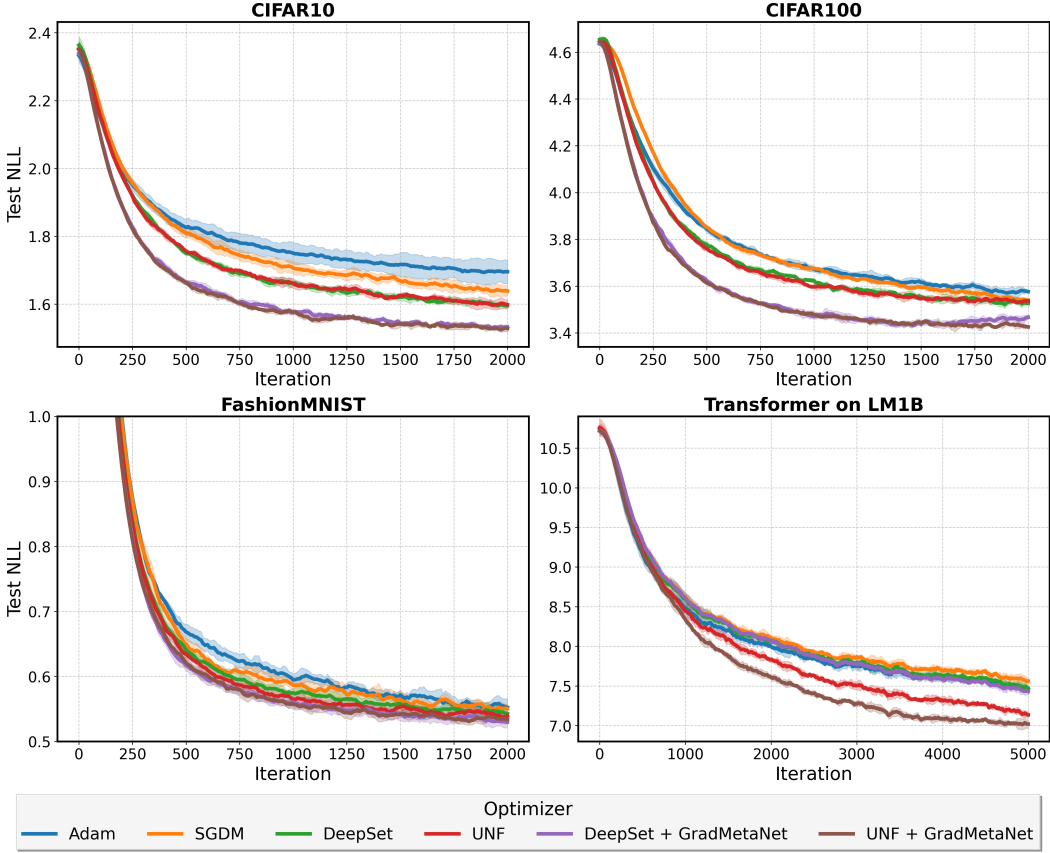


Figure 9: Test loss curves for MLP image classification tasks and a transformer language model trained on LM1B, using different optimizers and (learning rate tuned) Adam. Curves are smoothed and averaged over 5 random initializations, with shaded regions representing standard deviation.

**Additional experimental details.** We train all methods for 150K steps using the AdamW [50] optimizer with a batch size of 64. We search over learning rates in  $\{0.01, 0.005, 0.0001\}$ . For ScaleGMN and GMN we use the official implementation provided in Kalogeropoulos et al. [38] with the same parameter configuration provided by the authors. We use the bidirectional variant (ScaleGMN-B, Kalogeropoulos et al. [38]) with 10 layers and a hidden dimension of 128. The DWS [60] network consists of 8 layers with 128 hidden features. Finally, GradMetaNet consists of 10 layers with 256 hidden features, while GradMetaNet++ uses 3 blocks with 8 heads and 64 hidden features.